FLUID SOURCES AND FLUID-WALLROCK INTERACTION IN REGIONAL ALTERATION AND IRON OXIDE-CU-AU MINERALISATION, EASTERN SUCCESSION, MT ISA BLOCK: INSIGHT FROM C, O AND Sr ISOTOPES

FLUID SOURCES AND FLUID-WALLROCK INTERACTION IN REGIONAL ALTERATION AND IRON OXIDE-CU-AU MINERALISATION, EASTERN SUCCESSION, MT ISA BLOCK: INSIGHT FROM C, O AND Sr ISOTOPES

7.1 INTRODUCTION

The Eastern Succession of the Mt Isa Inlier has been at the forefront of research into the role of intrusives in the genesis of iron-oxide-Cu-Au mineralisation. While it is now becoming evident that some of the district's Cu-Au mineralisation is not synchronous with voluminous intrusion, and may be metamorphogenic in origin (e.g. Osborne deposit; Rubenach et al., 2001), most deposits are broadly synchronous with emplacement of the Williams and Naraku batholiths (e.g. Ernest Henry and Mt Elliott deposits). Various researchers in the Eastern Succession have attributed post-peak metamorphic regional alteration and Cu-Au mineralisation to saline fluids derived from predominantly magmatic sources (e.g. de Jong and Williams, 1995; Rotherham, 1997; Perring et al., 2000; Baker et al., 2001). Variations in fluid chemistry and metasomatic mineral assemblages have been argued to be the result of unmixing of H_2O-CO_2-NaCl fluids (Pollard, 2001) as well as progressive fluid-wallrock interaction (Oliver et al., in revision).

In other districts evaporite sequences and playa lakes have been invoked as the principal sources of saline ore fluids, and intrusives are thought to have acted as heat engines driving fluid flow (e.g. Barton and Johnson, 1996; Haynes et al., 1995). Elsewhere, contemporaneous intrusions have not been recognized and alternate fluid and heat sources seem plausible (e.g. Wernecke breccias, Yukon; Thorkelson et al., 2001). Clarifying the role of intrusive bodies in the genesis of iron-oxide-Cu-Au mineralisation is of direct relevance in assessing the prospectivity of greenfields terranes, and in establishing terrane specific exploration criteria.

Arguments for igneous fluid sources for regional alteration and Cu-Au mineralisation in the Eastern Succession have been based in large part on stable isotope data (e.g. Oliver et al., 1993; Rotherham, 1997; Perring et al., 2000; Baker et al., 2001). However, as pointed out by Haynes (2000), where hydrothermal flow paths are long, fluid isotopic signatures may equilibrate with host rock signatures,

rendering interpretation of fluid source from isotopic data ambiguous. Also, generalized isotopic ranges for different rock types and fluid sources commonly overlap, further complicating the interpretation of fluid sources.

This contribution presents a compilation of new and previously published carbon, oxygen and strontium isotope data from carbonate minerals in regional host-rocks and alteration assemblages, Zn-Pb-Ag mineralisation and iron-oxide related Cu-Au mineralisation in the Eastern Succession. Petrographic observations, cathodoluminescence images, and carbonate mineral chemistry support the isotopic data. Examining multiple isotopic systems (i.e. $\delta^{13}C + \delta^{18}O \pm {}^{87}Sr/{}^{86}Sr$) from a variety of host rocks and metasomatic assemblages has allowed for the characterization of different isotopic reservoirs that are specific to the Eastern Succession. This approach has removed much of the ambiguity associated with interpretation of single isotope systems, and in comparing data with generalized isotopic ranges for various rock or fluid types. In addition to clarifying sources for metasomatic fluids, the data sheds light on the nature of the fluid flow regime during metasomatism and the effects of fluid-wallrock interaction, as well as speculated links between iron-oxide-Cu-Au and Zn-Pb±Ag mineralisation.

7.1.1 Regional Geology

The Eastern Succession of the Proterozoic Mt Isa Block, northwest Queensland (Fig. 7.1), can be subdivided into the Cloncurry District and Mary Kathleen Fold Belt (MKFB), both of which preserve 100 km-scale fossil hydrothermal systems (e.g. Oliver et al., 1993; de Jong and Williams, 1995). Notably, iron-oxide-Cu-Au mineralisation is better developed in the Cloncurry District (e.g. Ernest Henry, Osborne, Eloise, Mt Elliott, Starra) than in the MKFB (e.g. Trekelano). Several aspects of the geology of the two regions of relevance to this contribution are briefly summarized here.

Supracrustal rocks in the Eastern Succession have been divided by Blake (1987) into Cover Sequences 1 (ca. 1870-1840 Ma), 2 (ca. 1790-1720 Ma) and 3 (ca. 1680-1620 Ma). Scapolitic calc-silicate rocks, marbles, meta-siltstones, and mafic and felsic meta-volcanic rocks of the Mary Kathleen Group (Cover Sequence

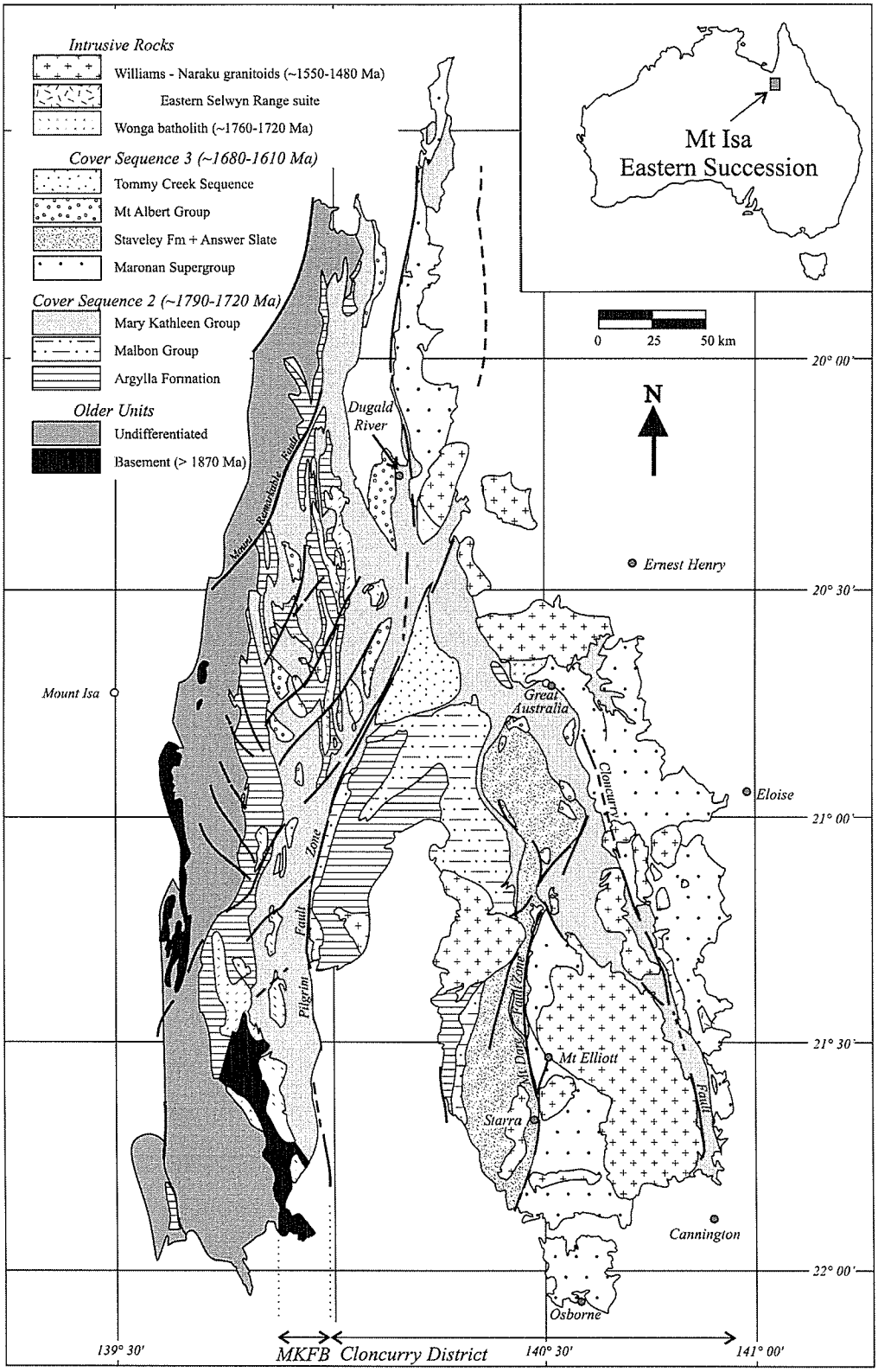

FIGURE 7.1.
Simplified geology of the Eastern Succession, Mt Isa Block, modified after Williams (1998).

2), including the Corella Formation, dominate the Mary Kathleen Fold Belt. The Burstall granite and associated mafic and felsic intrusives were emplaced during Wongan extension (ca. 1750 to 1730 Ma). Intrusion was synchronous with widespread sodic-(calcic) alteration, and Oliver et al. (1994) invoked dissolution of evaporitic sequences as a source of salt during this metasomatic event. Upright, north-trending folds and associated axial planar fabrics (D_2 and D_3 regionally; Oliver et al., 1991) accompanied amphibolite facies peak metamorphism at ca. 1575 Ma (Hand and Rubatto, 2002) and retrograde metamorphism. Extensive syn- to post-peak metamorphic fluid flow was predominantly focussed through breccia- and fracture-networks localized within brittle-ductile shear zones, and along contacts between Corella Formation meta-sedimentary rocks and pre-metamorphic Wonga-aged intrusions and adjacent skarns (Oliver and Wall, 1987; Oliver et al., 1990). Large-aperture calcite-rich veins, hydrothermal breccias and associated albite-actinolite-rich sodic-(calcic) alteration characterize the cores of these metasomatic systems. Spatially restricted intrusions show mutually cross-cutting relationships with these structural and metasomatic features.

The Cloncurry District (Fig. 7.1) is dominated by Corella Formation marbles and calc-silicate rocks (Cover Sequence 2), siliciclastic meta-sediments and mafic volcanics, including the Soldiers Cap Group (Cover Sequence 3), and granitoids of the Williams and Naraku batholiths (ca. 1550-1500Ma). Upper greenschist to amphibolite facies peak metamorphism occurred at ca. 1600-1584 Ma (Page and Sun, 1998; Giles and Nutman, 2002). Syn-peak metamorphic, tight to isoclinal folds exhibit a range of orientations due to strain partitioning during folding and subsequent reorientation of folds. Post-peak metamorphic brecciation is far more widespread than in the MKFB, and is in part a result of heterogeneous folding of Corella Formation stratigraphy that was fractured and boudinaged both before and during retrograde deformation (see **Chapter 4**, this study). More discrete fault- and granite carapace-breccias are also common and have acted as conduits for significant fluxes of metasomatic fluid at ca. 350° to >500°C (e.g. de Jong and Williams, 1995).

7.1.2 Theoretical background, sampling and analytical procedures

Carbon and oxygen isotope ratios

Carbon and oxygen stable isotope results from the Eastern Succession include data from regional host rocks and alteration in the Mary Kathleen Fold Belt and Cloncurry District, as well as data from ore deposits and prospects. Photographs of representative samples are presented in Figure 7.2. Carbon and oxygen isotope ratios are reported relative to V-PDB and V-SMOW respectively. All analyses were performed on carbonate minerals (calcite and subordinate dolomite and siderite) from both mixed carbonate-silicate ± oxide-sulphide powders, and hand-picked or micro-drilled pure carbonate samples. Direct comparison of data from calcite, dolomite and siderite is justified as the minerals show small fractionations at high temperatures. At the temperatures of interest (within approximately 300° and 600°C), fractionation between the minerals is not expected to exceed ca. 1‰ for either oxygen or carbon (e.g. Ohmoto and Rye, 1979; Golyshev et al., 1981; Zheng, 1999).

Calcite or dolomite precipitated from an isotopically homogenous H_2O-CO_2 fluid at 300°C would record $\delta^{13}C$ and $\delta^{18}O$ values greater by no more than approximately 1 and 4‰ respectively, than if precipitated from the same fluid at 600°C (fractionation factors from Ohmoto and Rye, 1979 and O'Neil et al., 1969). These values can be taken as an approximation of the maximum temperature effects on fractionation relevant to this study. Post-precipitation, low temperature isotopic equilibration with other minerals may also result in similar isotopic shifts.

Data from Mary Kathleen Fold Belt regional host rocks and alteration assemblages is summarized in Table 7.1, and is predominantly from Oliver et al. (1993; n=84), Cartwright (1994; n=79) and Cartwright and Oliver (1994; n=50) with additional unpublished data collected for this study (n=9). Data from Cloncurry District regional host rocks and alteration assemblages (Table 7.2) is unpublished and was collected for this study (n=97) and by Hingst (2002; n=6). Analyses in the MKFB and Cloncurry District datasets were preformed on calcite samples at Monash University on Finnigan MAT Delta E and MAT 252 mass spectrometers, with CO_2 extracted from calcite by reaction with 100% phosphoric

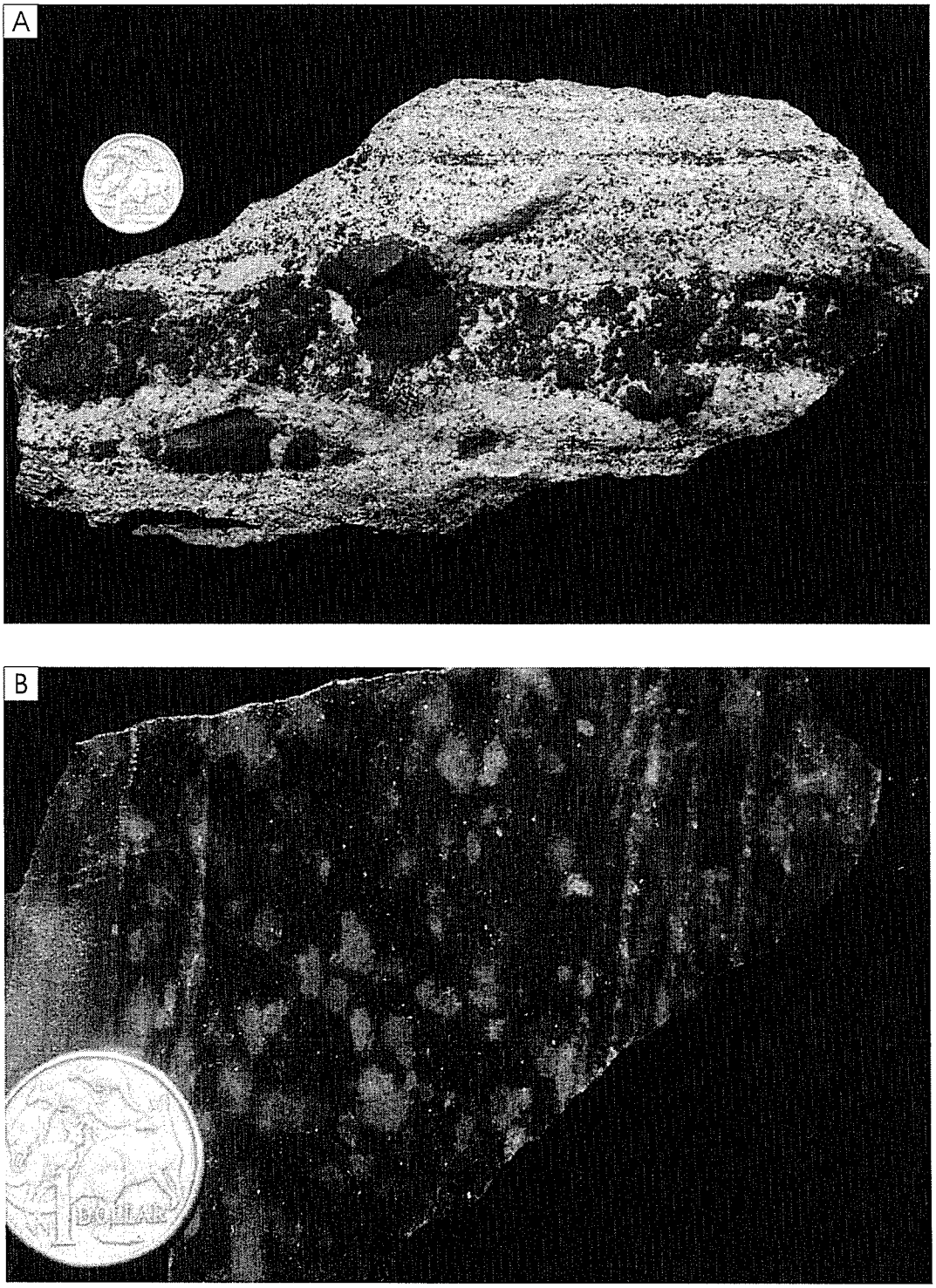

FIGURE 7.2.
Photographs of representative samples analyzed for this study. Diameter of coin in each photo is 2.4cm. (a) Corella Formation marble, with fractured and boudinaged meta-siltstone layer. (b) Unaltered, calcite-biotite-K-feldspar-scapolite-rich calc-silicate rock. Continued on following page.

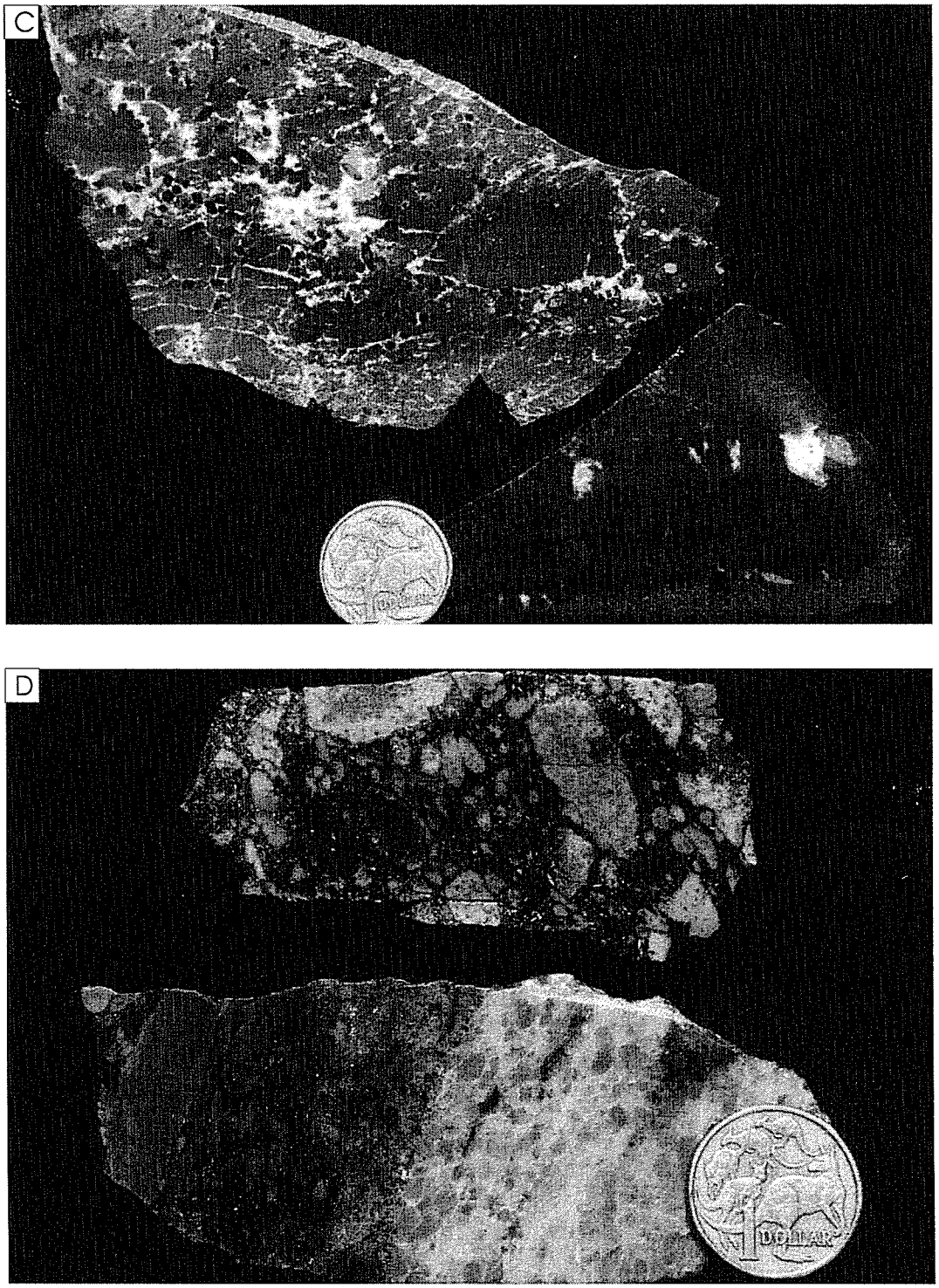

FIGURE 7.2. (continued)
(c) Scapolitic calc-silicate rocks with "rock-buffered" calcite veins, lacking visible alteration. (d) Na-(Ca) altered breccias, with albite- and actinolite-rich matrix and albitised clasts. Lower sample is cut by a calcite-rich vein. Continued on following page.

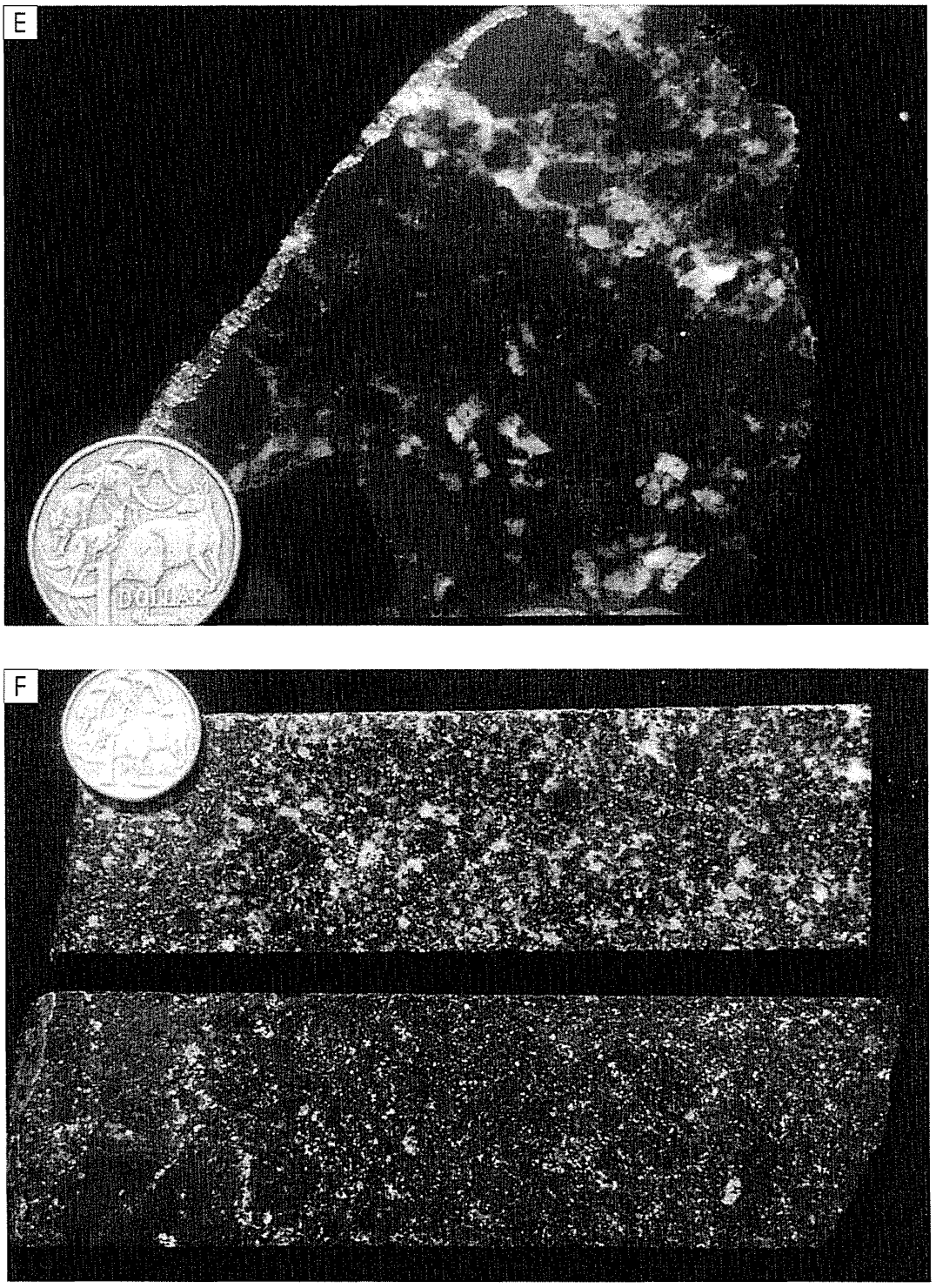

FIGURE 7.2. (continued)
(e) Retrograde, chlorite-bearing breccia with large component of calcite infill (white). (f) Infill- and matrix-supported Ernest Henry ore breccia.

acid at 25°C (McCrae, 1950). Precision on in house standards was approximately ±0.1‰, while repeat analyses of some samples yielded variations of several per mil, interpreted to reflect heterogeneity of isotopic ratios within selected samples (see below).

Data from ore deposits, prospects and their surrounds is compiled from a variety of published and unpublished sources (Table 7.3; n=301) as well as new data collected for this study (n=30). The compiled data was analyzed at a number of different laboratories, and it was not possible to cross-check results between laboratories. However, all data was collected following the method of McCrea (1950), and reported precision from in-house and international standards is ±0.1 to 0.2‰. Deposit data collected for this study was analysed at Monash University along with samples described above for the Cloncurry and MKFB datasets.

Strontium isotopes

Strontium isotope analyses were performed at the University of Adelaide on carbonate-rich samples that were crushed and homogenized prior to analysis, and had previously been analysed for carbon and oxygen isotopes. For each sample, approximately 200mg of material was leached in 4ml 1M ammonium acetate for 10 minutes in an ultrasonicator, in order to remove non-lattice Rb. The samples were subsequently rinsed and centrifuged in deionized water before dissolving overnight in 4ml 1M acetic acid in order to dissolve only the carbonate component of the samples. Samples were centrifuged and rinsed 3 times and each leachate then split into two aliquots. One aliquot was used for $^{87}Sr/^{86}Sr$ analysis, carried out on a Finnigan MAT262 thermal ionisation mass spectrometer. The remaining aliquot was spiked with an ^{84}Sr spike solution (0.86ppm Sr, 81.3% ^{84}Sr) and an ^{85}Rb spike solution (5.4ppm Rb, 99.5% ^{85}Rb) for analysis of Sr and Rb concentrations by isotope dilution with the measurements carried out on Finnigan MAT262 (Sr) and MAT261 (Rb) mass spectrometers.

Cathodoluminescence and mineral chemistry

Cathodoluminescence (CL) images were acquired by means of digital photography on an ELM-3R Luminoscope at the University of Alberta, operating at conditions of ca. 50 mtorr, 10-15Kv and 0.5-1.0 mA. CL images were used for textural observations, and as templates to guide carbonate chemistry analyses. Chemical analyses were performed along line traverses using a Jeol JXA-840 microprobe at James Cook University, analyzing 5 μm spots for 40 seconds. Element maps were collected using wavelength dispersive spectrometry (WDS).

7.2 CARBON and OXYGEN STABLE ISOTOPES

7.2.1 Mary Kathleen Fold Belt

Burstall Granite: ca. 1750-1730 Ma

Cartwright and Oliver (1994) and Cartwright (1994) presented carbon and oxygen stable isotope ratios from Corella Formation calc-silicate rocks and marbles in the Mary Kathleen Fold Belt (Fig. 7.3). The samples are from rocks that were metasomatised to scapolite-clinopyroxene-garnet-rich mineral assemblages during emplacement of the Burstall Granite and associated contact metamorphism (ca. 1750-1730 Ma). In both studies Corella Formation rocks exhibit marked shifts in $\delta^{18}O$ values from ca. 21‰ in least altered samples to ca. 11‰ $\delta^{18}O$. The authors interpreted the large depletions in $\delta^{18}O$ ratios, without significant shifts in $\delta^{13}C$ ratios, as marking infiltration by H_2O-rich, CO_2-poor (or -absent) fluids.

MKFB, high-temperature, Na-(Ca) alteration: ca. 1530-1520 Ma

Carbon and oxygen isotope data from large aperture, high temperature (400-600°C) calcite-dominated veins and associated sodic-(calcic) alteration in Corella Formation marbles, calc-silicate rocks and meta-dolerites in the Mary Kathleen Fold Belt has been described by Oliver et al. (1993). Veining, brecciation and alteration were focussed at contacts between units marked by significant competence contrasts and within brittle-ductile shear zones that cut peak-metamorphic structures. Albite- and actinolite-rich alteration assemblages replace peak metamorphic mineral assemblages and were formed predominantly at ca. 1530-1520 Ma, based on U-Pb

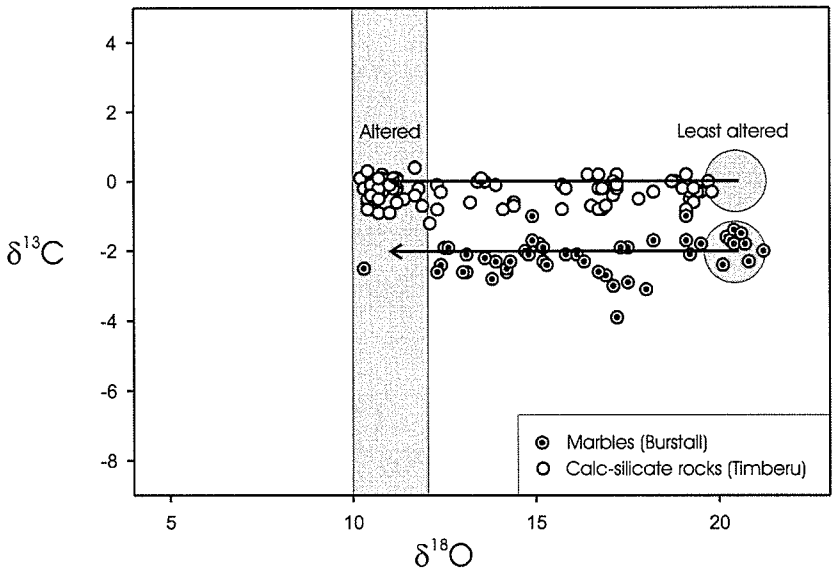

FIGURE 7.3.
Carbon and oxygen isotope data from MKFB marbles and calc-silicate rocks metasomatised during emplacement of the Burstall granite at ca. 1750-1730 Ma. Arrows and shaded fields in this and subsequent figures are drawn to highlight isotopic ranges and trends specific to data presented in this contribution.

titanite geochronology (Oliver et al., in revision). Isotopic ratios from the cores of the large calcite veins cluster at ca. 11‰ $\delta^{18}O$ and –7‰ $\delta^{13}C$, while smaller calcite veins and altered breccias record isotopic ratios ranging up to ca. 15.5‰ $\delta^{18}O$ and –2‰ $\delta^{13}C$ (Fig. 7.4). Least altered wallrocks record isotopic ratios of ca. 21‰ $\delta^{18}O$ and –1‰ $\delta^{13}C$. Additional samples collected for this study from MKFB large aperture vein systems also cluster at ca. 11‰ $\delta^{18}O$ and –7‰ $\delta^{13}C$, confirming the validity of comparing the two datasets.

The MKFB calcite veins are clearly out of isotopic equilibrium with their immediate wallrocks and Oliver et al. (1993) invoked externally derived metasomatic fluids of magmatic origin to explain the depleted isotopic values. Alternatively, isotopic fluid signatures may have been equilibrated with igneous rocks earlier in their flow path, although this seems unlikely for various reasons (see discussion). L-shaped trends in the isotopic data imply alteration by H_2O-CO_2 fluids that were nonetheless oxygen-rich and carbon-depleted relative to the calcareous wallrocks. Notably, this inferred fluid composition differs from fluids described above at ca. 1750-1730 Ma that lacked a significant CO_2 component.

MKFB, retrograde breccias and veins: <1530-1520 Ma (?)

Oliver et al. (1993) also presented limited data from medium to low temperature (epidote- and chlorite-bearing respectively) veins and breccias that record $\delta^{18}O$ signatures (ca. 6 to 10‰) that are depleted relative to the earlier, high temperature veins described above (Fig. 7.4). Similar depleted $\delta^{18}O$ values are reported here for calcite from the Mt Philp breccias in the Mary Kathleen Fold Belt. The retrograde breccias and veins, including the Mt Philp breccias, are characterized by pervasive red coloration due to fine hematite dusting and K-feldspar alteration. The shifts to lower $\delta^{18}O$ values cannot be explained by a decrease in temperature, as this would result in an increase in the $\delta^{18}O$-calcite values, relative to the higher temperature vein systems. Thus, depleted $\delta^{18}O$ values likely reflect the input of isotopically lighter fluids.

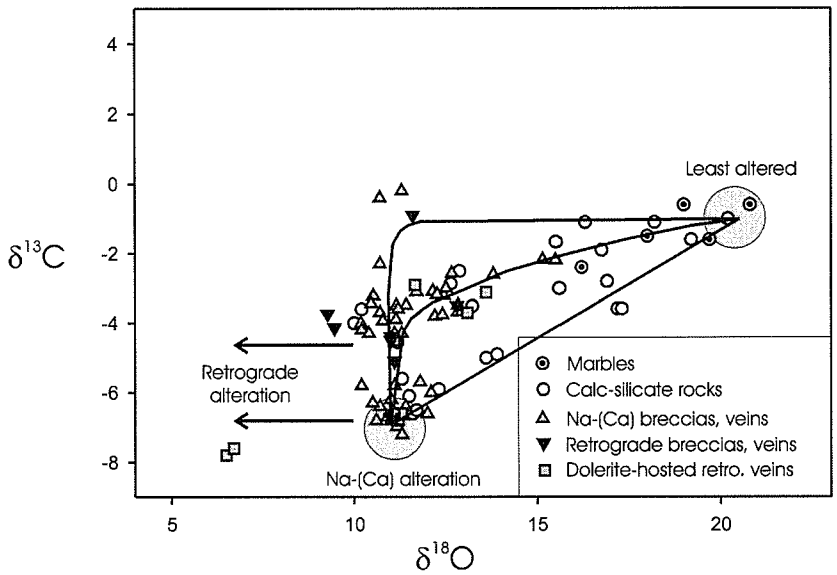

FIGURE 7.4.
Carbon and oxygen isotope data from late to post-peak metamorphic metasomatic systems in the MKFB records equilibration between unaltered marbles and calc-silicate rocks, and fluids responsible for albite-actinolite-rich alteration. Minor shifts to $\delta^{18}O$ values below ca. 10‰ are coincident with low temperature mineral assemblages, and record a distinct CO_2-poor, $\delta^{18}O$ depleted fluid source, possibly of meteoric origin. Arrows represent observed data variations as opposed to model curves.

7.2.2 Cloncurry District

Cloncurry District, high-temperature, Na-(Ca) alteration systems: ca. 1530-1520 Ma (?)

Breccias and veins associated with sodic-(calcic) alteration were collected within the Corella Formation and equivalent lithologies of the Cloncurry District, and are characterized by albite, actinolite and calcite ± clinopyroxene, magnetite, quartz, scapolite, biotite, titanite and apatite mineral assemblages. Calcite occurs as infill in veins and breccias, and as altered breccia matrix. The absolute timing of alteration is loosely constrained, with existing U-Pb titanite dates in the 1530-1520 Ma range, coincident with similar alteration in the MKFB (Oliver et al., in revision). The samples are characterized by intense bleaching of wallrocks and breccia clasts due to pervasive albitisation. Carbon and oxygen isotopic data forms a distinct cluster at 11‰ $\delta^{18}O$ and –7‰ $\delta^{13}C$, with spread towards higher carbon, and both higher and lower oxygen values (Fig. 7.5). Notably, the cluster at 11‰ $\delta^{18}O$ and –7‰ $\delta^{13}C$ is coincident with data from similar alteration systems described above in the MKFB. Again, these values are out of isotopic equilibrium with their hostrocks, implying externally-derived metasomatic fluids.

Cloncurry District, retrograde breccias and veins: <1530-1520 Ma (?)

Retrograde breccias and veins are characterized by calcite and chlorite ± quartz, hematite, K-feldspar and biotite mineral assemblages and lack actinolite or significant albite alteration. Calcite occurs as both infill and alteration of breccia matrix. The breccias and veins are commonly located within dilational fault zones, and are marked by bright-red coloration due to associated hematite dusting and K-feldspar alteration (K-feldspar alteration confirmed by GADDS analysis). The samples define an array from approximately 4 to 12‰ $\delta^{18}O$, and approximately -0.7 to –1.6‰ $\delta^{13}C$ (Fig. 7.5).

Cloncurry District, transitional breccias and veins

Transitional breccias and veins are characterized by similar mineralogy to sodic-(calcic) breccias and veins, but with the presence of significant chlorite ± K-

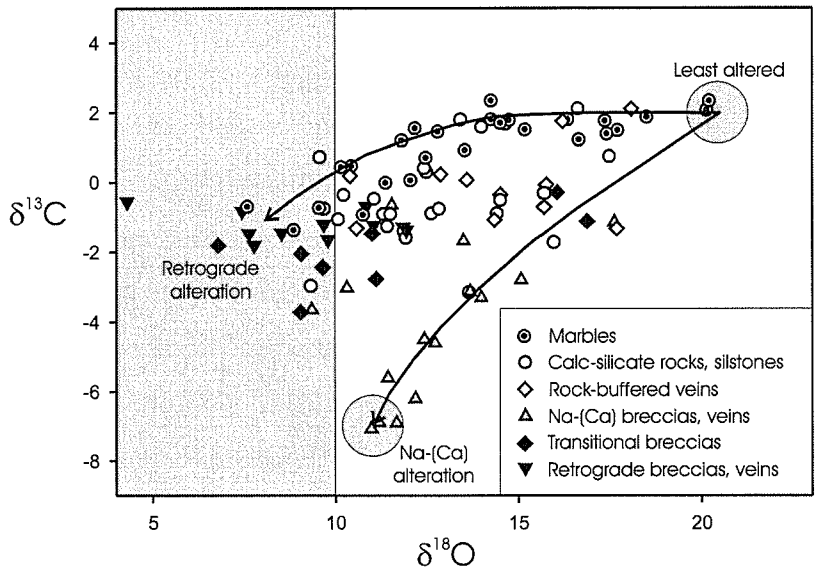

FIGURE 7.5.
Carbon and oxygen isotope data from the Cloncurry District records equilibration between unaltered marbles and calc-silicate rocks, and fluids responsible for albite-actinolite-rich alteration and retrograde chlorite-bearing alteration. Arrows represent observed data variations as opposed to model curves.

feldspar, hematite and hematite-dusting of feldspars. In some samples, the inferred lower-temperature chloritic assemblages clearly replace inferred higher temperature actinolitic assemblages, and likely record a separate, lower temperature fluid flow event. In other samples, chlorite and actinolite appear to be coeval. As might be expected, the isotopic data forms an array that falls between the sodic-(calcic) and retrograde samples (Fig. 7.5).

Cloncurry District, marbles, calc-silicate rocks and meta-siltstones

Least altered marbles within the Corella Formation contain >50% calcite and variable components of quartz, biotite, K-feldspar and scapolite. Altered samples also contain variable proportions of chlorite, actinolite, albite, magnetite, hematite, muscovite and tourmaline. In outcrop and in hand-sample, the marbles rarely exhibit macroscopic fracturing, however, adjacent meta-siltstones and calc-silicate rocks are commonly fractured and/or boudinaged. The marble data forms a curved array from approximately 20.5 to 8‰ $\delta^{18}O$ and 2 to -1‰ $\delta^{13}C$ (Fig. 7.5). The least depleted isotope signatures are from samples that lack chlorite or actinolite, and isotopic values from these samples are consistent with little altered, metamorphosed Proterozoic marine carbonates (e.g. Valley, 1986). These samples contain predominantly clean, polygonal calcite grains with smoothly curved boundaries. Samples with the most depleted isotopic signatures contain significant chlorite and fine-grained hematite dusting of calcite as well as irregular-shaped calcite grains with very abundant twins (commonly curved) and irregular and mottled grain boundaries.

Coarse-grained white to pink calcite commonly occurs in strain shadows adjacent to calc-silicate or meta-siltstone boudins within the marbles, and several analyses of this material have been included here. In most cases, coarse grained calcite in strain shadows has more depleted carbon and oxygen isotopic ratios than in adjacent fine- to medium-grained marble calcite, and may be inferred to reflect a greater component of externally derived carbon and oxygen precipitated in the strain shadows. However, in some cases, the inverse is true, implying a complex fluid flow history.

Least altered Corella Formation calc-silicate rocks and meta-siltstones have variable proportions of calcite (<50%), quartz, biotite, scapolite, K-feldspar, titanite and magnetite. Isotopic ratios for least altered samples range from approximately 17‰ $\delta^{18}O$ and 1.5‰ $\delta^{13}C$ to isotopically lighter ratios (Fig. 7.5). Where cut by veins and breccia bodies, calc-silicate rocks and meta-siltstones are progressively altered to albite-actinolite- or chlorite-rich mineral assemblages, and show corresponding depletions in calcite $\delta^{18}O$ and $\delta^{13}C$, as low as approximately 9.3 and –3‰ respectively (Fig. 7.5).

Cloncurry District, rock-buffered veins

Rock-buffered veins are defined by calcite ± quartz and biotite infill assemblages that lack mesoscopic evidence for associated wallrock alteration, and are in apparent mineralogical equilibrium with least altered Corella Formation lithologies. While the veins cannot be attributed to a distinct metasomatic event, they cut peak metamorphic fabrics and mineral assemblages. Isotopic analyses from rock-buffered veins overlap with analyses from least altered marbles, calc-silicate rocks and meta-siltstones (Fig. 7.5).

Cloncurry District, carbonaceous metasediments

Relative to samples from within the Corella Formation, calcite samples from calcareous lithologies and vein and breccia infill within the Soldiers Cap Group exhibit depleted $\delta^{13}C$ values as low as –13.2‰ (Fig. 7.6). These depleted carbon isotopic ratios are interpreted to reflect partial equilibration between metasomatic fluids and graphitic meta-sediments, which are common in the Soldiers Cap Group. Although the $\delta^{13}C$ signature of calcareous pelitic rocks in the Soliders Cap is poorly constrained, data from the Dugald River deposit indicates $\delta^{13}C$ values of ca. –18‰ for carbonates within black shales. As such, $\delta^{13}C$ values reported here for veins within the Soldiers Cap appear to have been only partially buffered by the veins' immediate host rocks.

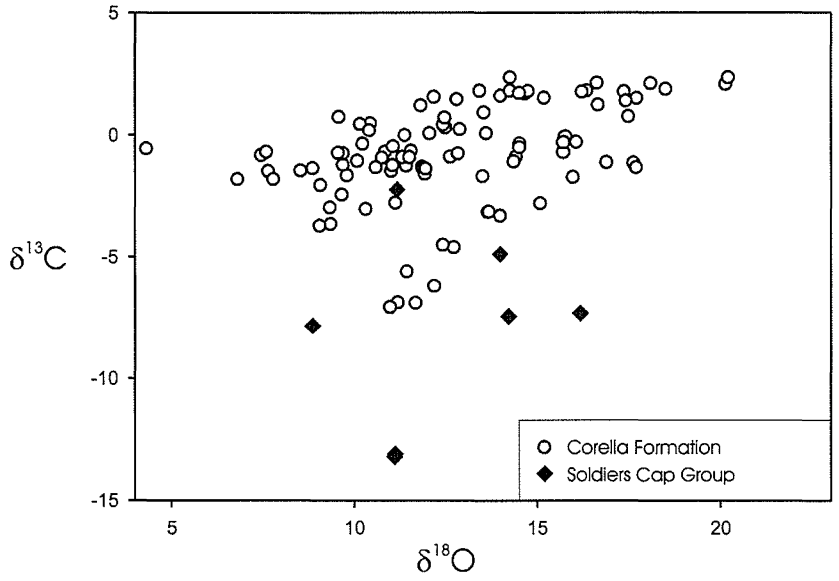

FIGURE 7.6.
Carbon and oxygen isotope data from calcareous and carbonaceous lithologies, and breccia and vein infill within the Soldiers Cap Group of the Cloncurry District records distinctly low $\delta^{13}C$ values relative to samples within the Corella Formation.

7.2.3 Cloncurry District and Mary Kathleen Fold Belt comparisons

The bulk of the carbon and oxygen isotopic data collected from regional host-rocks and post-peak-metamorphic alteration in the Cloncurry District and Mary Kathleen Fold Belt defines a three-endmember array (Fig. 7.7). These endmembers correspond with 1) calcite in isotopic equilibrium with least altered marbles and calc-silicate rocks, 2) fluids responsible for high temperature albite-actinolite-rich Na-(Ca) alteration, and 3) retrograde chlorite-hematite-bearing alteration. Thus, the bulk of available carbon and oxygen stable isotope data in these districts is interpreted to reflect interaction between two isotopically distinct metasomatic fluids and marine meta-carbonates. In the Cloncurry District, shifts towards lower $\delta^{13}C$ values (below –7‰) are inferred to reflect interaction of metasomatic fluids with graphitic meta-sediments common within Cover Sequence 3 (Fig. 7.6). This interaction is under-represented in the available datasets as a result of sample collection having been focussed within Cover Sequence 2, and the relative scarcity of carbonates within Cover Sequence 3.

Na-(Ca) alteration

Isotopic values for calcite associated with albite- and actinolite-rich sodic-(calcic) alteration in both the MKFB and Cloncurry District strongly cluster around the same value (Fig. 7.7). This, together with similarities in mineralogy, structural style, and structural timing suggests a widespread metasomatic event with a similar fluid source (or sources) and similar fluid pathways in both the Cloncurry District and MKFB. Further, the strong clustering of data at 11‰ $\delta^{18}O$ and –7‰ $\delta^{13}C$ indicates that in the cores of the large sodic-(calcic) alteration systems, isotopic signatures were strongly fluid-buffered with respect to both $\delta^{18}O$ and $\delta^{13}C$. As demonstrated by Oliver et al. (1993) these values are clearly out of isotopic equilibrium with local wallrocks, and are most consistent with a magmatic fluid source, although fluids that were equilibrated with isotopically homogenous igneous rocks are also possible. This distinction is addressed further in the discussion.

In the Cloncurry District, isotopic data combined with field and map observations (Figs. 4.2 and 6.5, this study) indicate that Na-(Ca) alteration

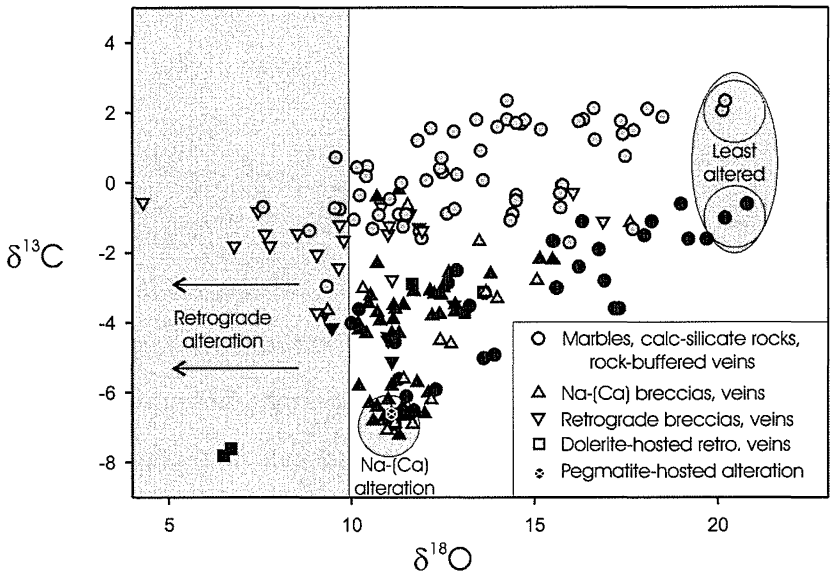

FIGURE 7.7.
Carbon and oxygen isotope data from regional host rocks and post-peak metamorphic alteration in the Corella Formation of the MKFB (black symbols) and Cloncurry District (grey symbols). Note the varying starting compositions for least-altered marbles and calc-silicates in the Cloncurry District versus the MKFB. Also note the coincident ratios for calcite associated with sodic-(calcic) alteration in both belts.

accompanied widespread brecciation. In areas of intense alteration, isotopic ratios and mineral assemblages are in clear disequilibrium with their immediate host rocks, and are considered to be "fluid buffered". Elsewhere, large areas are affected by weak or diffuse alteration with "rock buffered" isotopic signatures and metasomatic assemblages approaching equilibrium with those of least altered metamorphic rocks. In contrast, in the MKFB, brecciation, veining and accompanying Na-(Ca) alteration are predominantly confined to narrow "fluid buffered" corridors within shear zones, and along contacts between units marked by major competence contrasts.

Retrograde alteration

In the available datasets, retrograde veins and breccias are more abundant in the Cloncurry District than the MKFB (Fig. 7.7). While this may to some degree be a function of sampling bias, regional alteration mapping (Oliver, unpublished data; **Chapter 6**, this study) indicates that retrograde red-rock alteration assemblages are far more widespread in the Cloncurry District than in the MKFB.

Metamorphic decarbonation and isotopic equilibration

In the Cloncurry District least altered marbles and calc-silicate rocks record isotopic ratios of ca. 20.5 ‰ $\delta^{18}O$ and 2‰ $\delta^{13}C$ (Fig. 7.7). In contrast, chemically similar (but higher metamorphic grade) least altered lithologies in the MKFB record isotopic ratios of ca. 20.5‰ $\delta^{18}O$ and –1‰ $\delta^{13}C$ (Fig. 7.7). While primary variations in isotopic ratios cannot be ruled out, the difference in carbon isotopic ratios between the belts may in part be a function of varying degrees of metamorphic decarbonation. Cloncurry District samples were metamorphosed to (biotite-zone) greenschist facies (e.g. Foster and Rubenach, 2001), and least altered samples lack amphibole or pyroxene. In contrast the MKFB samples were metamorphosed to amphibolite facies, and most samples contain metamorphic amphibole and/or clinopyroxene. Upper temperature limits of ca. 550°C and 650°C are likely for the northern Cloncurry District and MKFB respectively (Oliver et al., 1991; Reinhardt, 1992; Hingst, 2002; Foster, pers. comm, 2003). Likely mineral

reactions in the MKFB between 550°C and 650°C reported by Oliver et al. (1992) include:

5 biotite + 6 calcite + 24 quartz 3 amphibole + 5 K-feldspar + 6 CO_2 + 2 H_2O
biotite +3 calcite + 6 quartz 3 cpx + K-feldspar + 3 CO_2 + H_2O
amphibole + 3 calcite + 2 quartz 5 cpx + 3 CO_2 + H_2O
3 amphibole + 6 calcite + K-feldspar 12 cpx + biotite + 6 CO_2 + 2 H_2O

The magnitude of depletion in $\delta^{13}C$ values for decarbonation reactions such as those given above has been calculated for both Batch and Rayleigh devolatization models at 550°C (Fig. 7.8), following equations outlined by Nabelek (1991), and using calcite-CO_2 fractionation factors of Ohmoto and Rye (1979). In order to explain the approximately 3‰ depletion in $\delta^{13}C$ values for least altered samples in the MKFB relative to the Cloncurry District, in excess of 65% of the carbon in the rocks at greenschist facies would have to be lost through lower amphibolite facies decarbonation reactions. While this is reasonable for presently calcite-poor MKFB calc-silicate rocks and meta-siltstones, it is unlikely for marbles that retain significant proportions of calcite. Alternatively, greater depletions in $\delta^{13}C$ can be expected if decarbonation reactions occur at lower temperatures. This may result from variable X_{CO2} and/or pressure differences during metamorphism.

An alterative mechanism for variations in $\delta^{13}C$ values for Corella Formation calcite in the Cloncurry District relative to the Mary Kathleen Fold Belt may be expected from shifts in $\delta^{13}C$ (calcite) values during thermally driven isotopic equilibration between carbonates and reduced carbon. At increasing metamorphic grade, carbon fractionation values ($\Delta_{calcite\text{-}graphite}$) record a narrower range, and smaller modal values (ca. 12‰ for low grade to greenschist facies metamorphism, vs. ca. 4‰ at amphibolite facies), reflecting an increasing in $\delta^{13}C$ graphite values and decrease in $\delta^{13}C$ calcite values (e.g. Des Marais, 2001).

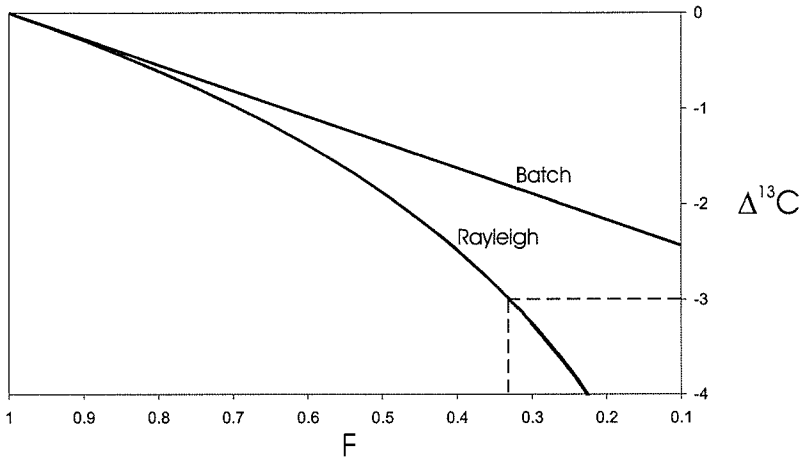

FIGURE 7.8.
Model curves for the depletion in carbon isotope values ($\delta^{13}C$) as a function of the percentage of carbon remaining in the rock after devolitization (F). Curves are calculated for Rayleigh and Batch decarbonation at 550°C. A 3‰ depletion in $\delta^{13}C$ would require loss of greater than 65% of the carbon in a given sample.

7.2.4 Zn-Pb-Ag mineralisation

Dugald River

The strata-bound, Dugald River Zn-Pb-Ag deposit (38Mt @ 13.0%Zn, 2.1%Pb and 42g/t Ag; Newberry et al., 1993) is hosted by a fault bound block of carbonaceous and calcareous Dugald Slates of the Lady Clayre Dolomite, within the Mount Albert Group (Cover Sequence 3). The Corella Formation forms the basement rocks to the deposit. Based on Pb isotope data, Gulson (1985) suggested that mineralisation at Dugald River has a similar age to Mt Isa Zn-Pb ores at ca. 1650 Ma. Based on isotopic, paragenetic and metal zonation data, Dixon and Davidson (1996) concluded that mineralisation at Dugald River formed during early diagenesis, and was upgraded during tectonism. In contrast, Xu (1997) used microstructural evidence to support an epigenetic origin for the deposit.

Dixon and Davidson (1996) presented extensive carbon and oxygen isotopic data from the deposit, which defines a linear array that can be divided into two endmember isotopic and geologic populations (Fig. 7.9). Analyses from the graphitic Footwall Limestone ($\delta^{13}C$ = -11 to -5‰) were interpreted by the authors to reflect metamorphic equilibration between marine carbonate and organic carbon. Analyses from the ore horizon and its immediate hostrocks were interpreted as recording oxidation of organic carbon. These analyses are amongst the lowest published $\delta^{13}C$ values from carbonates in the Eastern Succession. A cluster of data at ca. 14‰ $\delta^{18}O$ and –18‰ $\delta^{13}C$ are here taken as being characteristic of carbonate in equilibrium with abundant organic carbon, and are used for comparison in subsequent plots. Additional isotopic data from Porter (1990) overlaps with near ore samples of Dixon and Davidson (1996), and extends to higher $\delta^{13}C$ values (up to –4‰; Fig. 7.9). This spread in data suggests an additional carbon and possibly oxygen source to the marine carbonate and organic carbon reservoirs documented by Dixon and Davidson (1996). One possibility is that theses samples record a fluid phase present during the remobilization of ore. Based on the available isotopic data, such a fluid could have been either magmatic or metamorphic in origin.

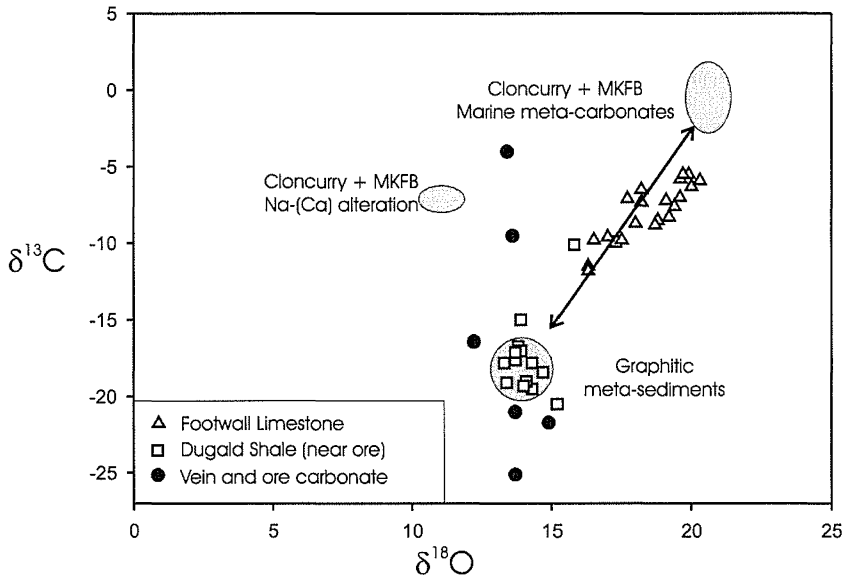

FIGURE 7.9.
Isotopic data from the Dugald River Zn-Pb-Ag deposit indicates marine meta-carbonates and graphitic meta-sediments are the principal sources of oxygen and carbon in the deposit and surrounds. Veins and (remobilised?) ore samples record an additional carbon and oxygen source that may be either metamorphic or magmatic. Arrow represents observed data variations as opposed to a model curve.

7.2.5 Cu-Au mineralisation

Cover Sequence 2

The only deposit hosted entirely within the Mary Kathleen Group for which carbon and oxygen isotopic data was available for this study is the Ernest Henry Cu-Au deposit (166Mt @ 1.1% Cu and 0.55ppm Au; Ryan, 1998). Isotopic data presented here is from Twyerould (1997), Mark et al. (1999) and this study. Variably sheared and brecciated Mt Fort Constantine felsic volcanics and subordinate calc-silicate rocks of the uppermost Mary Kathleen Group dominate hangingwall stratigraphy at the deposit. The footwall to the deposit is dominated by a calcite-rich, intensely sheared unit termed "marble matrix breccia" by Ernest Henry Mining geologists. Mark et al. (1999) interpreted the marble matrix breccia as consisting predominantly of infill calcite. In contrast, in **Chapter 5** it was argued based on textural similarities with Cloncurry District marbles that the marble matrix breccia is indeed a marble, albeit intensely sheared and metasomatised.

The $\delta^{18}O$ and $\delta^{13}C$ signature of carbonate in equilibrium with the Mt Fort Constantine felsic volcanics is poorly constrained, but is expected to approach values typical of other igneous rocks at ca. 10 and –5‰ respectively. However, the volcanics contain negligible carbon, and as such the $\delta^{13}C$ ratio of metasomatic carbonate at the deposit would be expected to be buffered by Corella Formation marine carbonates, and/or a metasomatic fluid, if that fluid contained appreciable carbon. The bulk of carbon and oxygen stable isotope data from Ernest Henry lies between the fields defined for calcite associated with Na-(Ca) alteration, and marine meta-carbonates in the Cloncurry District and MKFB (Fig. 7.10). While $\delta^{18}O$ (calcite) values at ca. 10-12‰ may reflect a component of oxygen sourced from local felsic volcanic rocks, many analyses in this range of $\delta^{18}O$ also record $\delta^{13}C$ signatures that are depleted relative to marine metacarbonates. This is best explained by calcite in isotopic equilibrium with a metasomatic fluid with $\delta^{13}C$ values similar to fluids associated with Na-(Ca) alteration. Some samples record shifts towards $\delta^{18}O$ (calcite) values as low as 1.3‰, indicating the input of an additional oxygen source, possibly in the form of meteoric water. However, the strong clustering of analyses at and greater than 11‰ $\delta^{18}O$ (calcite) suggests that

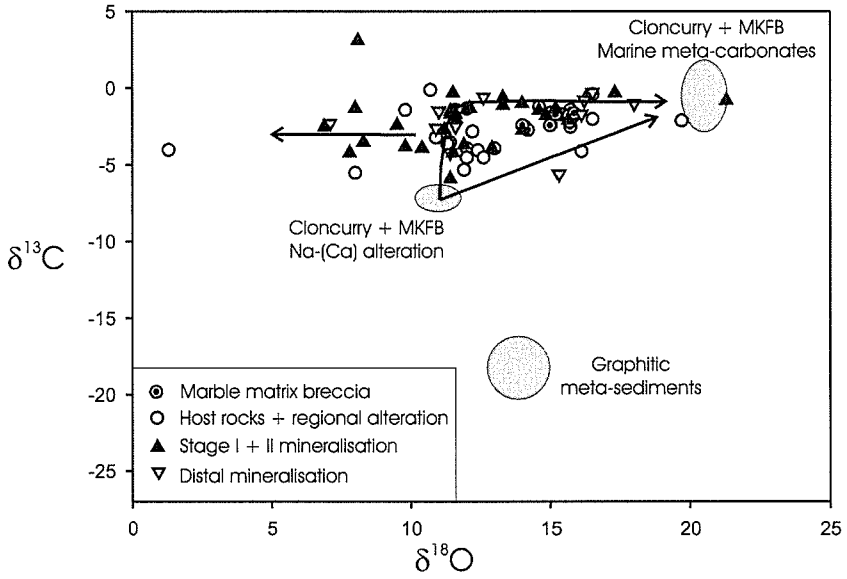

FIGURE 7.10.
The bulk of the carbon and oxygen isotopic data from Ernest Henry is consistent with oxygen and carbon being sourced from Corella Formation marine meta-carbonates, and fluids similar to those responsible for regional sodic-(calcic) alteration. L-shaped curves imply that fluids were H_2O-rich, but contained some CO_2. Shifts to $\delta^{18}O$ values below ca. 10‰ record a small component of isotopically light fluid. Arrows represent observed data variations as opposed to model curves.

this low $\delta^{18}O$ source contributed only a small component of oxygen to the deposit. Further, cathodoluminescence work indicates that a cooler fluid was introduced at least in part after the main mineralizing event (see below). This late fluid may have resulted in the observed shifts towards lighter $\delta^{18}O$ signatures.

Cover Sequences 2 and 3

Great Australia is a small Cu-Au-Co deposit hosted by Toole Creek Volcanics (TCV) of the Soldiers Cap Group (Cover Sequence 2), adjacent to and within a splay of the Cloncurry fault that marks a sheared contact with Corella Formation marbles and calc-silicate rocks to the west. The deposit contains a supergene resource of 1.7 Mt @ 1.2% Cu, with a larger undefined hypogene orebody (Cannell and Davidson, 1998). Isotopic data reported by Davidson and Garner (1997) and Cannell and Davidson (1998) from Great Australia shows a wide range in both $\delta^{18}O$ and $\delta^{13}C$ ratios (Fig. 7.11). A cluster of analyses at ca. 10‰ $\delta^{18}O$ and –6‰ $\delta^{13}C$ is similar to values at 11‰ $\delta^{18}O$ and –7‰ $\delta^{13}C$ for albite-actinolite-rich breccias and veins in both the Cloncurry District and MKFB, and may imply a similar fluid source. Another cluster at ca. 17.5‰ $\delta^{18}O$ and –5‰ $\delta^{13}C$ approaches values typical of little-altered marbles and calc-silicate rocks and likely reflects partial isotopic equilibration between a metasomatic fluid and Corella Formation stratigraphy within or adjacent to the Cloncurry Fault zone. Additional samples from Great Australia record depleted $\delta^{13}C$ values of ca. –16‰ and are inferred to record interaction between metasomatic fluids and graphitic metasediments within the Soldiers Cap Group.

Cover Sequence 3

Carbon and oxygen stable isotope data on carbonates is available from numerous Cu-Au deposits and prospects within Cover Sequence 3 of the Eastern Succession (Fig. 7.12). The data includes analyses from altered and unaltered host rocks as well as metasomatic assemblages. The bulk of the data lies within a broadly triangular three-endmember field. Endmember ratios are consistent with being in equilibrium with 1) marine meta-carbonates, 2) graphitic meta-sediments

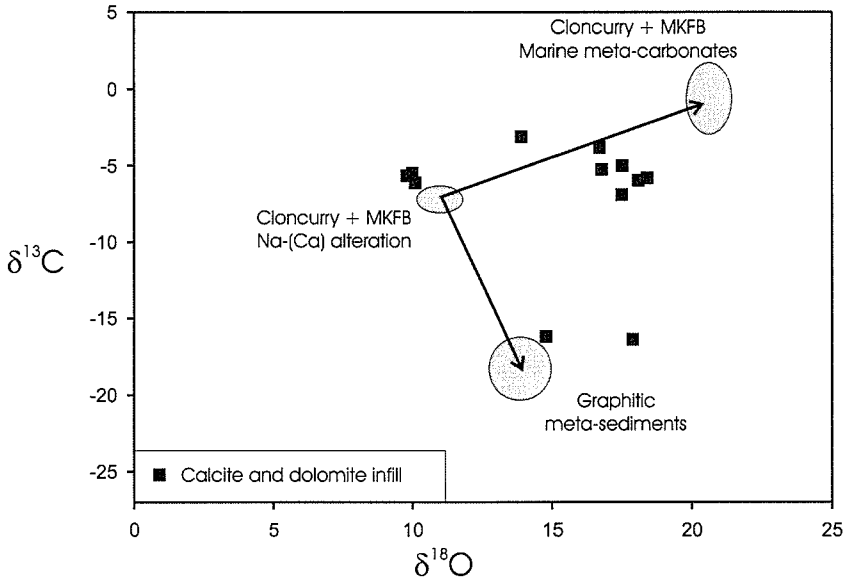

FIGURE 7.11.
Isotope data from the Great Australia Cu-Au deposit records interaction between a fluid that is isotopically similar to that responsible for regional sodic-(calcic) alteration, marine meta-carbonates, and graphitic meta-sediments. Arrows represent observed data variations as opposed to model curves.

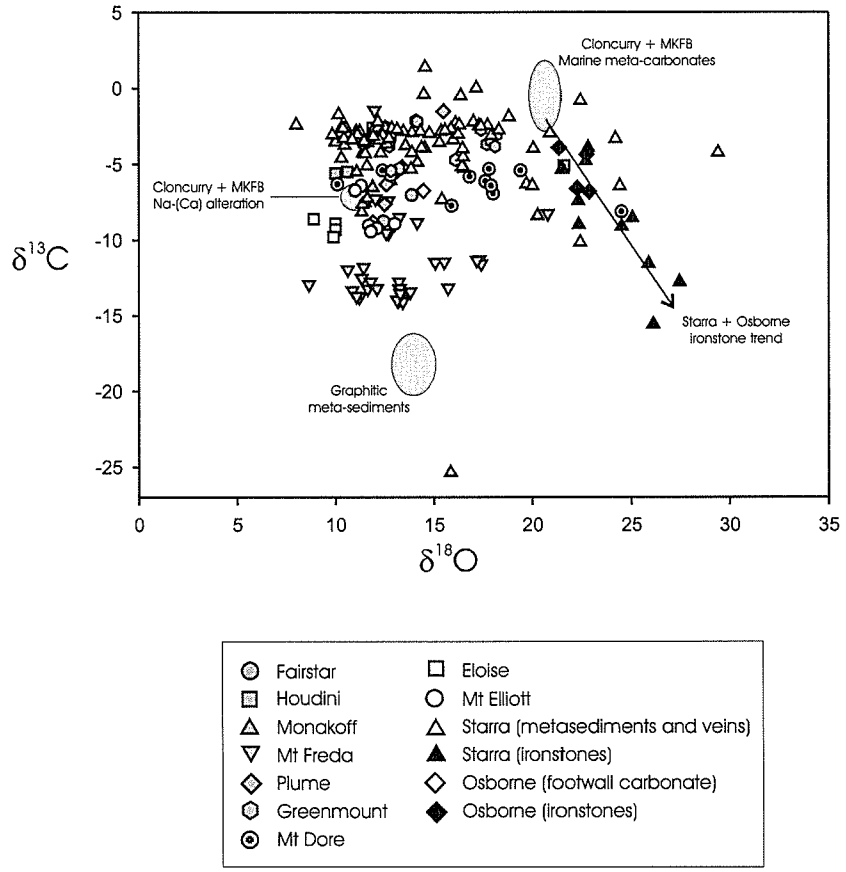

FIGURE 7.12.
Carbon and oxygen stable isotope data from Cu-Au deposits hosted within Cover Sequence 3 predominantly lies between fields defined for sodic-(calcic) alteration, marine meta-carbonates and graphitic meta-sediments. The Starra and Osborne ironstones define a separate trend, implying a distinct, likely non-magmatic fluid source. Arrow represents observed data variations as opposed to a model curve.

and 3) metasomatic fluids with isotopic signatures similar to fluids responsible for sodic-(calcic) alteration. While both marine meta-carbonates and graphitic meta-sediments are locally abundant within Cover Sequence 3 stratigraphy, in some cases isotopic shifts towards marine meta-carbonate values likely record equilibration with Mary Kathleen Group stratigraphy (Cover Sequence 2), prior to mineral precipitation within Cover Sequence 3.

Mineralisation at Starra is hosted by magnetite-rich ironstones that pre-date introduction of Cu and Au. The origin of the ironstones is contentious, with syngenetic (e.g. Davidson, 1989) and epigenetic (e.g. Rotherham, 1997) origins having been proposed. Williams et al. (2001) documented fluid chemistries that differ markedly between the ironstones and Cu-Au mineralisation, and suggested that several distinct metasomatic fluids are recorded at the deposit. Notably, the majority of Br/Cl ratios reported by Williams et al. (2001) for the ironstones fall outside of fields defined for modern magmatic fluids.

The bulk of carbon and oxygen isotope data from both mineralized and barren veins and metasedimentary rocks at the Starra deposit lies between fields defined for marine metacarbonates and fluids responsible for sodic-(calcic) alteration (Fig. 7.12). Thus, mineralisation at Starra can be explained by precipitation from metasomatic fluids that were isotopically similar to those responsible for sodic-(calcic) alteration, but that equilibrated to varying degrees with carbonate-bearing meta-sedimentary rocks. In contrast, data from ironstones at the Starra deposit extends from values in equilibrium with marine meta-carbonates to higher $\delta^{18}O$ and lower $\delta^{13}C$ values. As suggested by Davidson (1989), the Starra ironstone trend likely reflects equilibration between a light $\delta^{13}C$, heavy $\delta^{18}O$ fluid and carbonates in the host sedimentary sequence. The source of such a fluid is unconstrained, but is clearly isotopically distinct from fluids responsible for either sodic-(calcic) or retrograde alteration in the Eastern Succession, as well as most other examples of iron-oxide and Cu-Au mineralisation.

Limited data from ironstones at Osborne also falls along the Starra ironstone trend, and was taken by Davidson (1989) to reflect a similar origin for magnetite at the two deposits. Recent geochronological and petrographic data suggest that iron-

oxide and Cu-Au mineralisation at Osborne occurred at ca. 1595 Ma (Gauthier et al., 2001; Rubenach et al., 2001), synchronous with the peak of metamorphism. No voluminous intrusions of this age are known in the Eastern Succession, and a metamorphosed or metamorphogenic origin for some ironstones at Osborne and Starra seems likely.

7.3 STRONTIUM ISOTOPES

$^{87}Sr/^{86}Sr$ ratios and Rb and Sr concentrations were analyzed from Cloncurry District marbles and sodic-(calcic) and retrograde breccias and veins, as well as the Ernest Henry marble matrix breccia and ore breccia, and a MKFB large aperture calcite vein associated with sodic-(calcic) alteration. As evident in Table 7.4, Rb concentrations in all samples are extremely low, and range from 0.02 to 1.02ppm. Because of these low Rb concentrations, present day $^{87}Sr/^{86}Sr$ ratios are likely to be only slightly changed from ratios at the inferred Proterozoic time of mineral precipitation (Table 7.4). Interpretations here have thus been based on measured $^{87}Sr/^{86}Sr$ ratios, rather than specifically calculating for ^{87}Sr produced by in situ decay of ^{87}Rb (e.g. Shields and Veizer, 2002).

Samples from the Cloncurry District reveal a narrow range in $^{87}Sr/^{86}Sr$ ratios between 0.7093 and 0.7223, whereas the one sample from the MKFB (sample T72c) has an anomalously high $^{87}Sr/^{86}Sr$ ratio of 0.7398. This sample was collected from the Tribulation large-aperture calcite vein that lies at the contact between Corella Formation marbles and calc-silicate rocks to the west, and meta-dolerite to the east (see **Chapter 5**, this study). The meta-dolerite was likely emplaced with the Burstall Granite at ca. 1750-1730 Ma, and such intrusions are far more common in the MKFB than the Cloncurry District. Page (1983b) presents initial $^{87}Sr/^{86}Sr$ ratios calculated for the Burstall Granite and associated rhyolite dikes that range from 0.714 to 0.780, and indicates that these rocks have been grossly isotopically disturbed since initial crystallisation. Based on the above observations, it seems likely that the radiogenic Sr signature from the Tribulation vein is in part inherited from fluid interaction with the older meta-dolerite. If this is accepted, then it would appear that the strontium isotopic composition of fluids at Tribulation were reset by

wallrock interaction much more rapidly than were fluid carbon and oxygen isotope signatures. This would be the expected situation if the fluids were strontium-deficient relative to their wallrocks.

Cloncurry District marble samples record relatively high Sr concentrations and low $^{87}Sr/^{86}Sr$ ratios between 0.7093 and 0.7111 (Fig. 7.13). The $^{87}Sr/^{86}Sr$ values are nonetheless substantially higher than values predicted for Proterozoic seawater (Shields and Veizer, 2002), indicating isotopic disturbance during diagenesis, metamorphism and/or metasomatism. The lowest recorded $^{87}Sr/^{86}Sr$ ratio of 0.7093 is from the apparently least altered marble analysed (as indicated by carbon and oxygen isotopes).

Analyses from calcite infill record lower Sr concentrations and elevated $^{87}Sr/^{86}Sr$ ratios (Fig. 7.13). The vein-forming fluids were clearly not in equilibrium with either seawater or Corella Formation marbles. An analysis from the Ernest Henry marble matrix breccia records a similar $^{87}Sr/^{86}Sr$ signature to calcite from sodic-(calcic) alteration assemblages, and likely indicates buffering of $^{87}Sr/^{86}Sr$ ratios by a similar metasomatic fluid source.

Strontium data from the Cloncurry District samples correlates well with $\delta^{18}O$ data, and confirms that the infill assemblages are out of isotopic equilibrium with Corella Formation marbles (Fig. 7.14). Notably, a single analysis from the Ernest Henry ore breccia has similar $^{87}Sr/^{86}Sr$ and $\delta^{18}O$ ratios to Cloncurry District retrograde breccias, and may indicate a similar fluid source. Alternatively, Ernest Henry is predominantly hosted by Mt Fort Constantine felsic volcanics of similar age to the Burstall Granite (ca. 1750-1730 Ma). These rocks may have provided a source of radiogenic strontium, in a manner similar to that proposed above for the Tribulation vein and not applicable to the other Cloncurry District samples.

7.4 CATHODOLUMINESCENCE AND CARBONATE CHEMISTRY

A cathodoluminescence (CL) investigation of calcite textures was undertaken to complement the isotopic data presented above. Microprobe traverses were also carried out to assess chemical variations corresponding with variations is CL response. Observations and data from marbles, vein and breccia infill associated

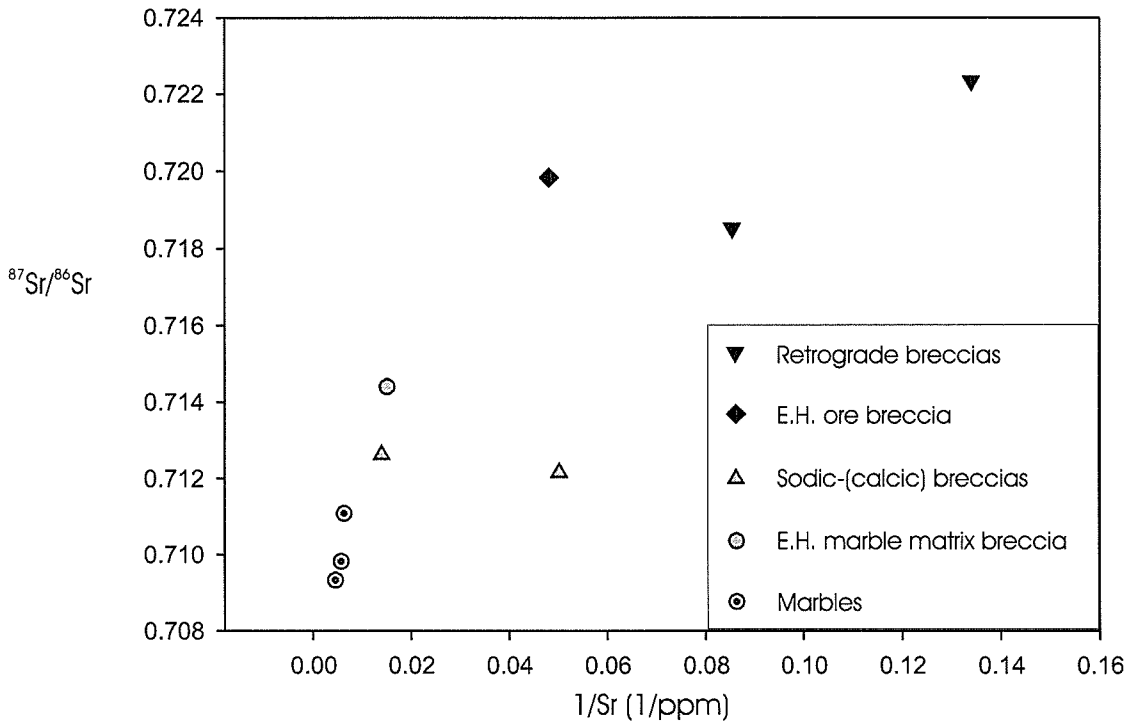

FIGURE 7.13.
Correlation diagram of $^{87}Sr/^{86}Sr$ vs. 1/Sr for Cloncurry District calcite samples. The inverse correlation between $^{87}Sr/^{86}Sr$ and Sr concentration reflects mixing between a Sr-rich, low $^{87}Sr/^{86}Sr$ marine carbonate reservoir, and a strontium-poor, high $^{87}Sr/^{86}Sr$ reservoir (or reservoirs). The more radiogenic strontium values are from vein and alteration calcite.

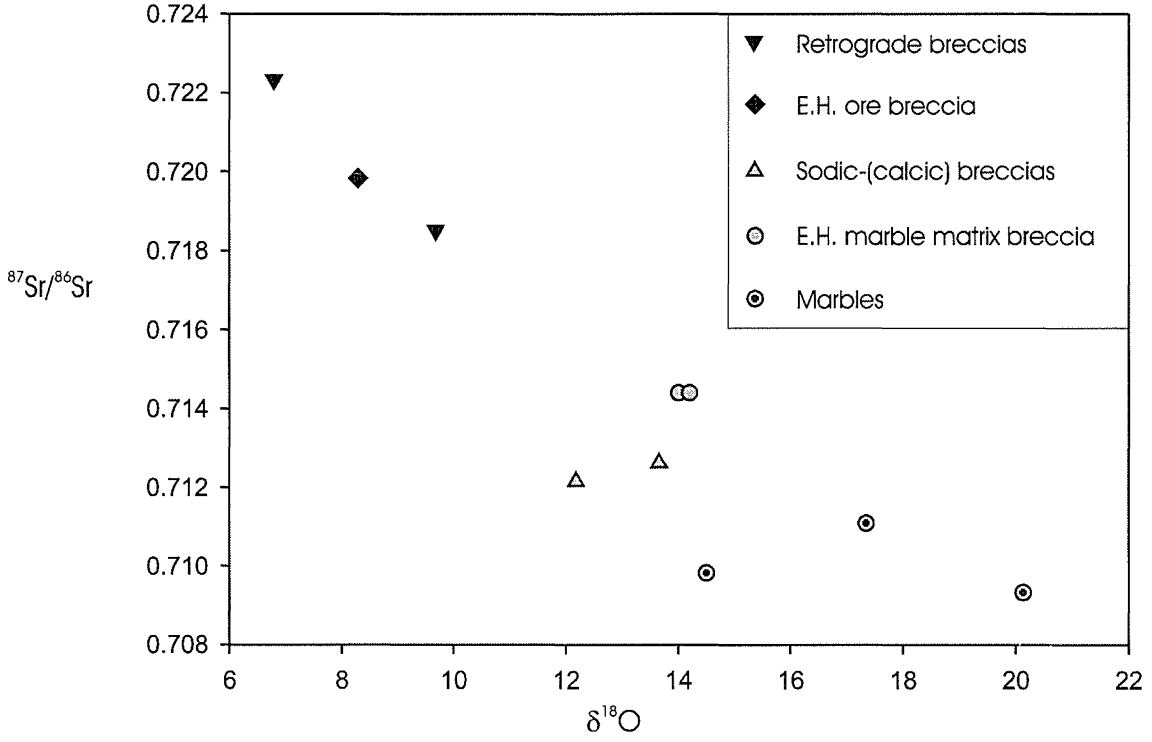

FIGURE 7.14.
$^{87}Sr/^{86}Sr$ vs. $\delta^{18}O$ ratios for Cloncurry District calcite samples indicate that infill calcite is enriched in radiogenic Sr, and depleted in $\delta^{18}O$ relative to Cloncurry District marbles.

with both albite-actinolite- and chlorite-hematite-rich alteration, as well as the Ernest Henry deposit are described here. Photomicrographs of textures commonly observed using cathodoluminescence are presented in Figure 7.15, and ternary diagrams of carbonate composition are given in Figure 7.16.

7.4.1 Marbles

Greenschist facies Cloncurry District marbles exhibit a range of textures visible in CL images that are not identifiable through conventional petrography, and that correspond well with isotopic trends. Where multiple isotopic analyses were performed from the same marble samples, isotopic ratios vary significantly within individual hand specimens (up to 6‰ $\delta^{18}O$ and 1‰ $\delta^{13}C$). The marbles investigated by CL imagery preserve dull orange-luminescing cores to calcite grains, commonly with an interconnected network of bright orange- to yellow-luminescing grain boundaries, twins and microfractures (Fig. 7.15a). The bright-luminescing calcite has a mottled texture in CL images, as a result of abundant fine-grained mineral inclusions (predominantly chlorite and hematite, see below). The network of bright luminescing calcite must post-date any significant recrystallisation of calcite grains during metamorphism and high temperature deformation, and is interpreted to record variations in trace element geochemistry as a result of metasomatism. If this is accepted, then the network of bright luminescing calcite records late- to post-metamorphic and -tectonic fluid pathways. A broad correspondence in the abundance of bright luminescing calcite and the degree of depletion in isotope signatures is noted, and the variability in isotopic signatures within individual samples is readily explained by the heterogeneous distribution of bright luminescing calcite.

Microprobe line traverses constrained by CL imagery were undertaken in order to characterize the chemical nature of the bright luminescing calcite network in Cloncurry District marbles. Figure 7.17 presents two CL images and associated microprobe traverses. Bright luminescing calcite is visible along grain boundaries, twins, and completely replacing some grains. Microprobe analyses indicate that dull luminescing calcite grain cores are characterized by very homogenous

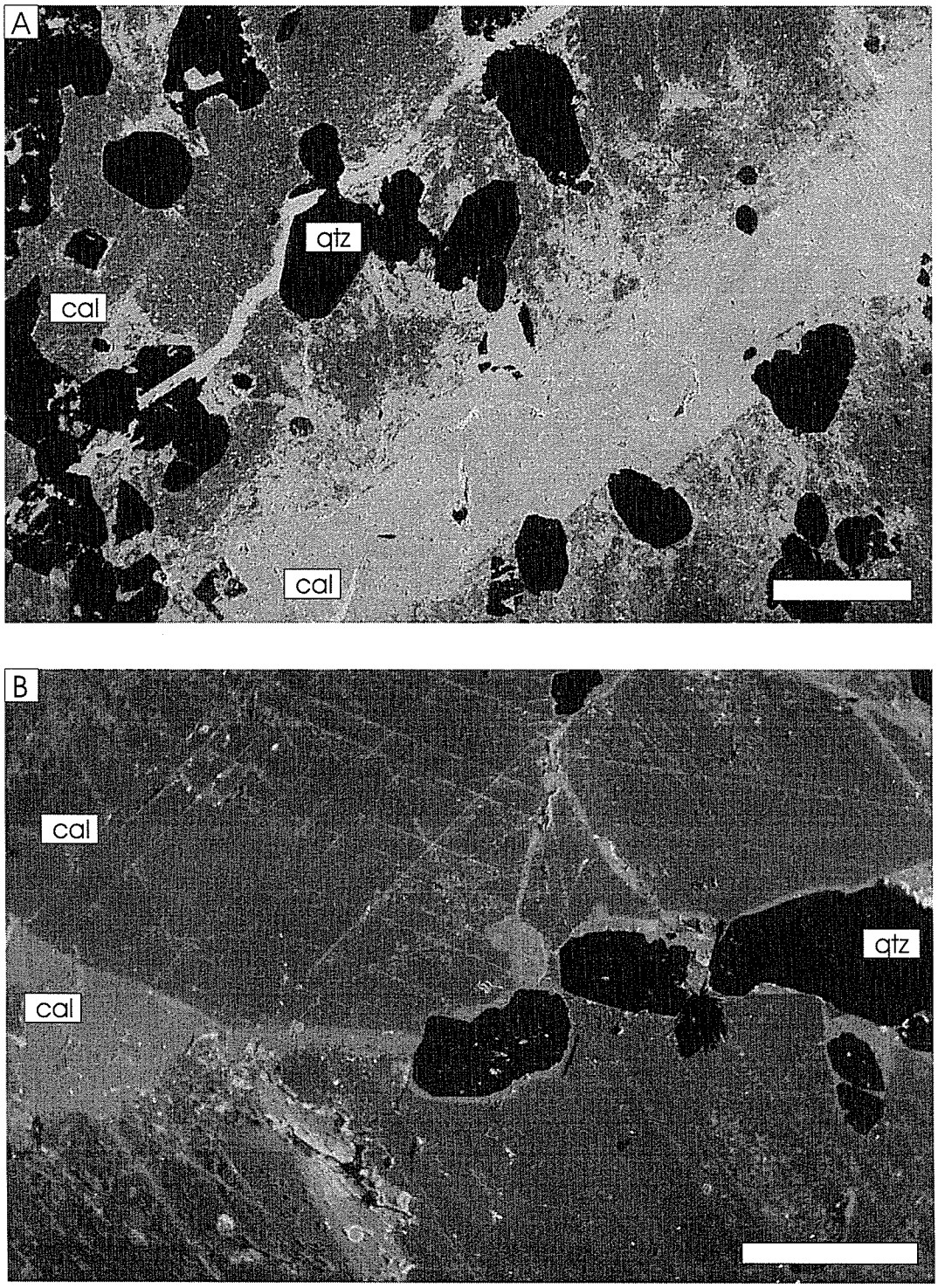

FIGURE 7.15.
CL images of textures commonly observed in Eastern Succession calcite grains. All scale bars are 500 microns. (a) Bright-luminescing calcite-microfractures in Cloncurry District marble are not visible in transmitted light, but common in CL images. (b) Predominantly homogenous medium to bright-luminescing infill calcite associated with albite-actinolite-rich alteration, shows some grain-boundary replacement by brighter luminescing calcite. Continued on following page.

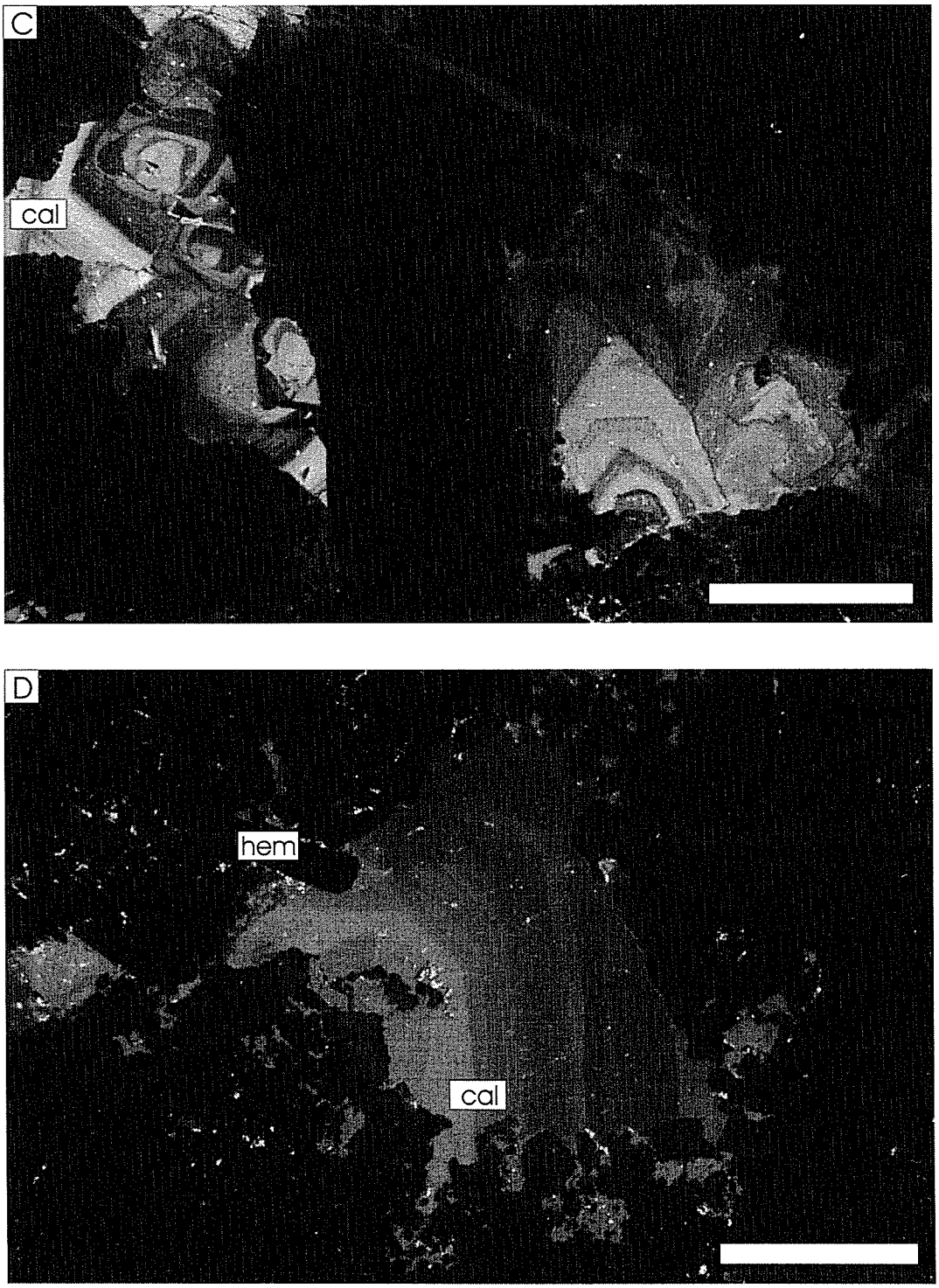

FIGURE 7.15. (continued)
(c-d) Infill in retrograde breccias and veins commonly preserves growth-banding, and in all cases lacks grain-boundary alteration. Continued on following page.

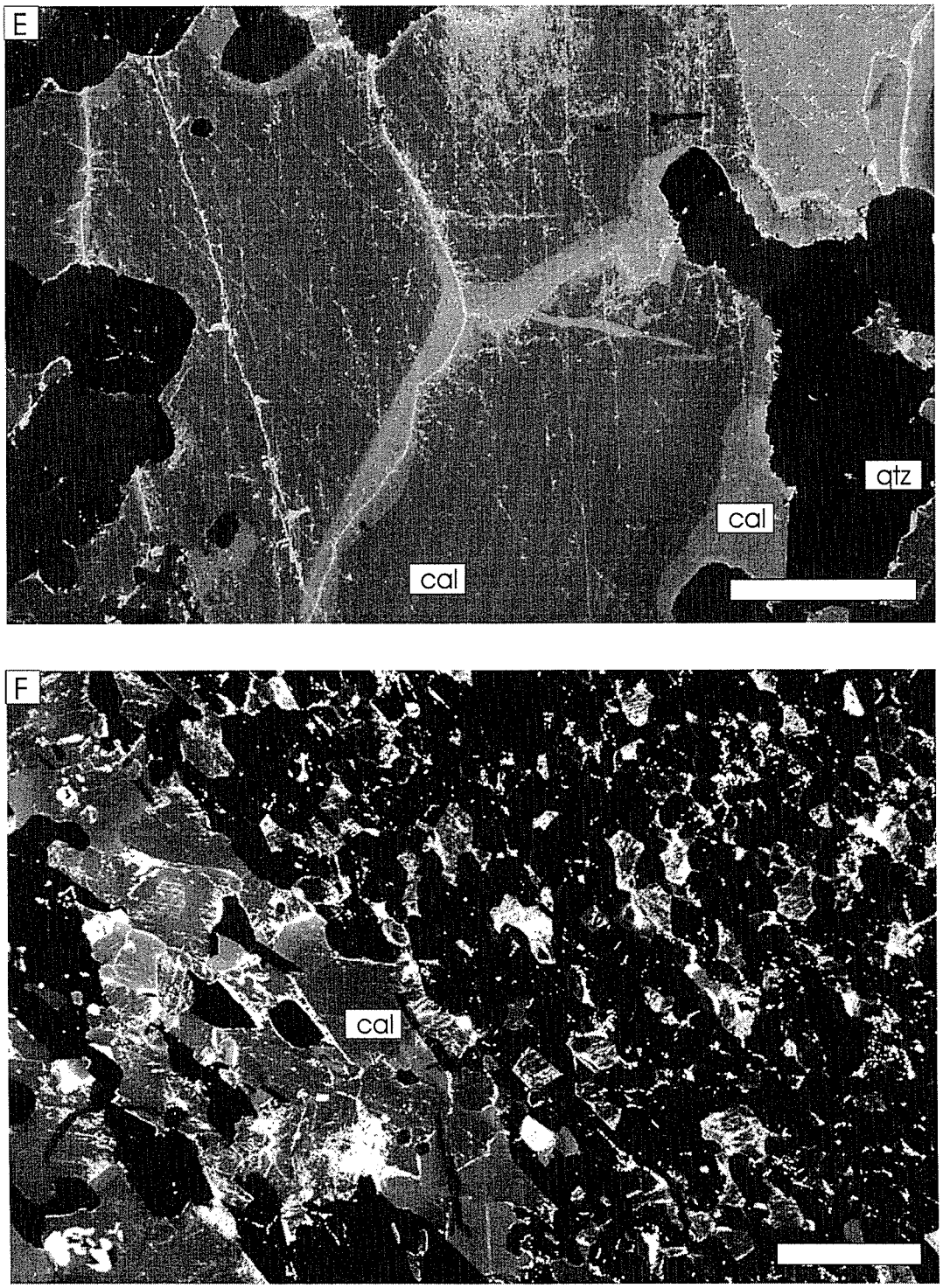

FIGURE 7.15. (continued)
Bright-luminescing calcite grain boundary alteration evident in (e) the Ernest Henry ore breccia and (f) the Ernest Henry marble matrix breccia.

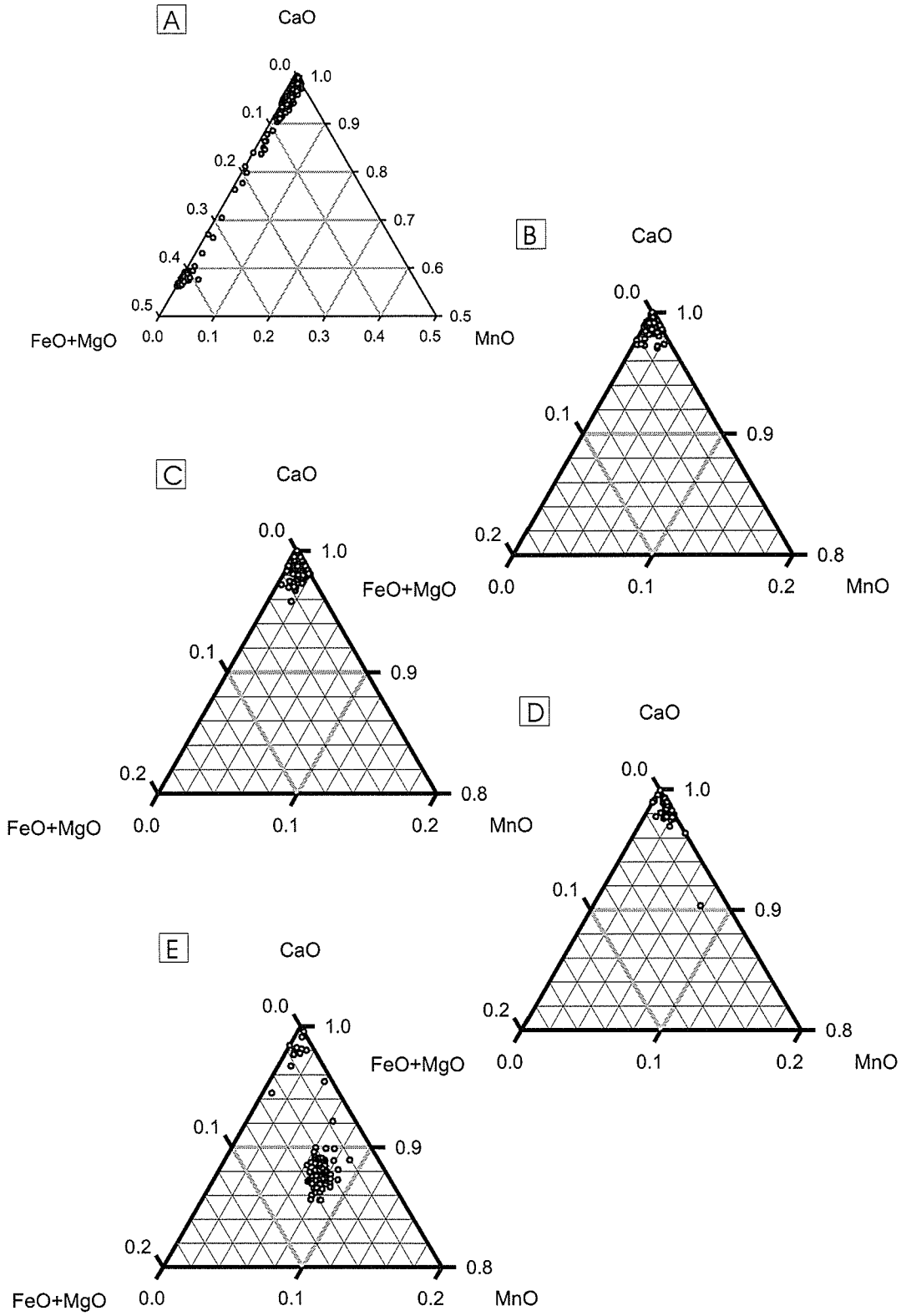

FIGURE 7.16.
Ternary diagrams illustrating the chemical range for carbonates in (a) Cloncurry district marbles, (b) sodic-(calcic) breccias and veins, (c) retrograde breccias and veins, (d) Ernest Henry ore breccia and (e) the Ernest Henry marble matrix breccia.

concentrations of MgO and FeO (total FeO + Fe_2O_3 analysed as FeO). Areas of bright luminescing calcite have slightly depleted background concentrations of MgO and FeO relative to dull-luminescing calcite, and include intermittent spikes in FeO ± MgO concentrations. These spikes are inferred to record small inclusions of hematite and chlorite giving the bright luminescing calcite its mottled appearance. Coarser grained hematite and chlorite have been identified in these samples petrographically. Chemical variations corresponding with the CL images are also evident in wavelength dispersive (WDS) microprobe element maps (Fig. 7.17), and confirm that in areas of bright luminescing calcite, MgO and FeO are stripped from calcite and concentrated into small mineral inclusions.

7.4.2 High temperature, sodic-(calcic) alteration systems

CL images from calcite breccia and vein infill associated with sodic-(calcic) alteration assemblages (albite-actinolite-rich) typically reveal homogenous, moderate to bright-luminescing calcite (Fig. 7.18). Zoning is weakly developed or more commonly absent, a feature that may indicate either stable fluid chemistry and P-T conditions during precipitation, or subsequent recrystallization. In some cases, infill calcite exhibits replacement by brighter luminescing calcite along grain boundaries and microfractures (Fig. 7.15b), with textures similar to those described above for marbles. This suggests some fluid flow after the main calcite precipitation event. However, networks of brighter luminescing calcite were not chemically distinguishable from the main episode of calcite infill, at the level of resolution provided by the microprobe. Microprobe traverses indicate that infill calcite associated with sodic-(calcic) alteration is chemically homogenous, with very low concentrations of FeO, MgO and MnO (Fig. 7.18a).

7.4.3 Retrograde breccias and veins

Calcite infill associated with retrograde (chlorite-hematite-bearing) breccias and veins commonly shows complex growth zoning in CL images, marked by alternating moderate- and bright-luminescing calcite (Figs. 7.15c,d and 7.18). These variations likely reflect small changes in the trace element chemistry of the calcite,

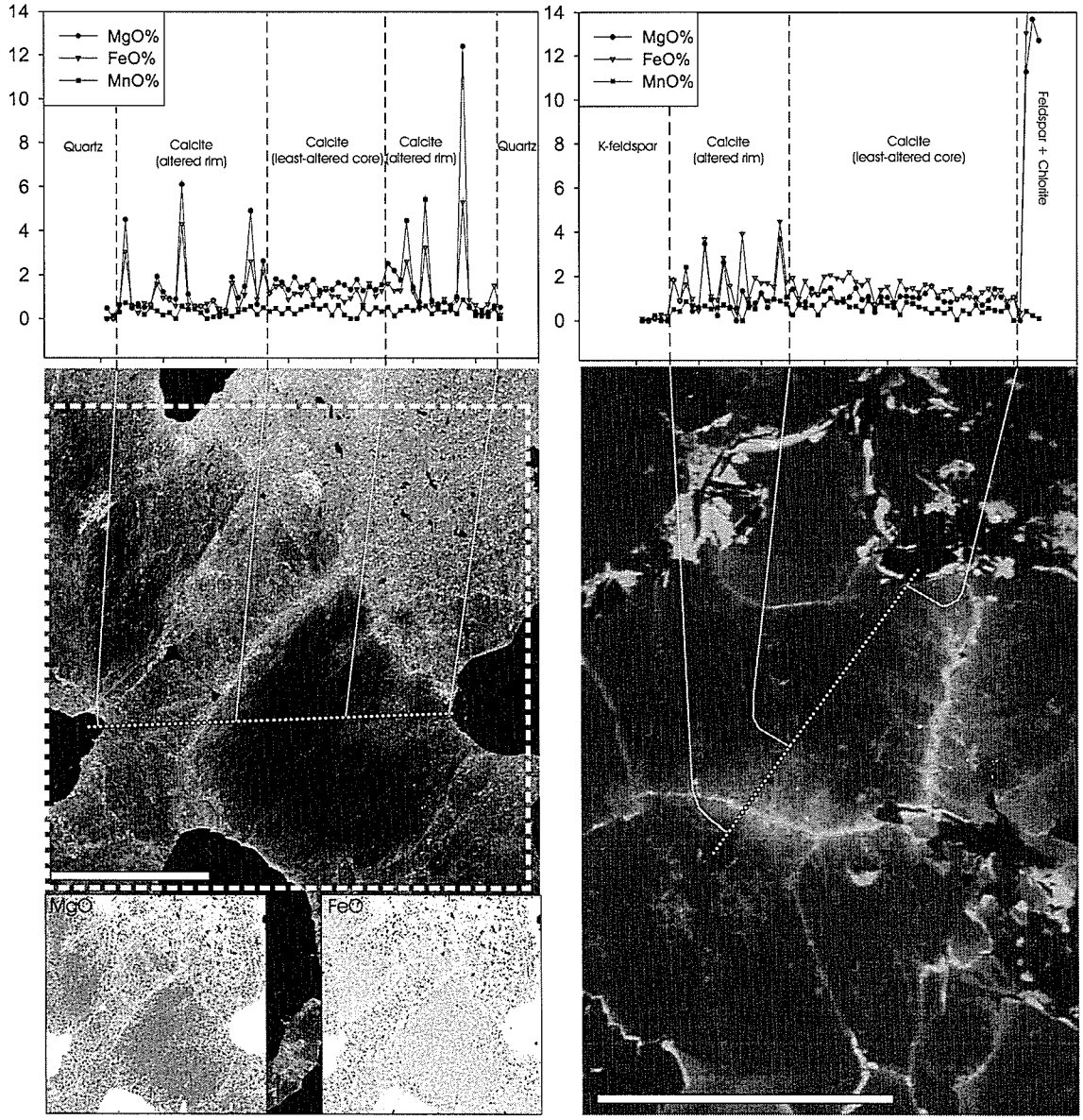

FIGURE 7.17.
CL images and associated microprobe traverse from Cloncurry District marbles. Bright-luminescing calcite networks are marked by redistribution of FeO and MgO from metamorphic calcite into fine-grained inclusions of chlorite and hematite (total Fe reported as FeO). Dashed square indicates the position of MgO and FeO WDS element maps (inset). Dark areas in element maps are enriched in MgO or FeO. Scale bars = 500 microns.

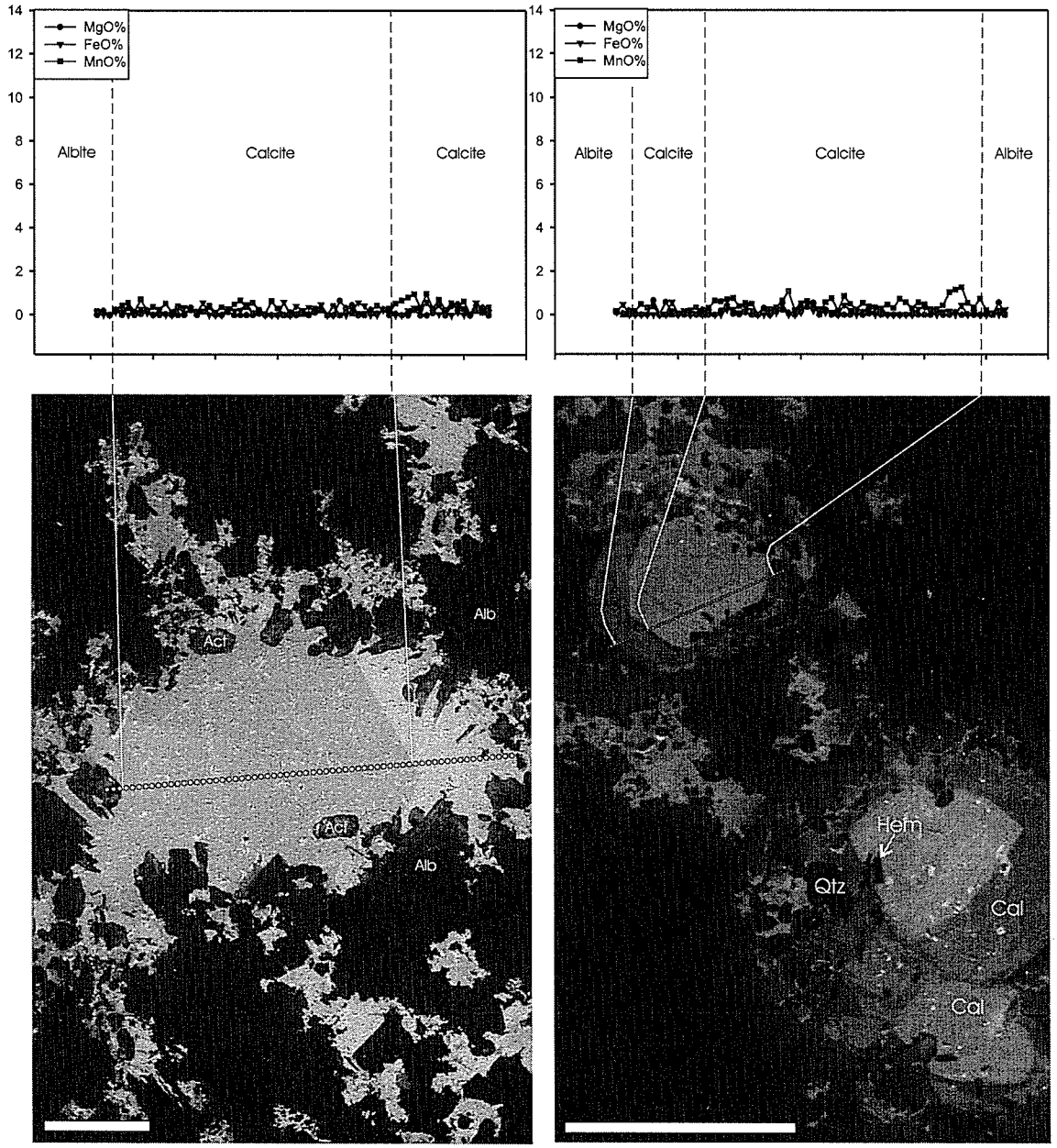

FIGURE 7.18.
CL images and microprobe traverses for calcite infill in both sodic-(calcic) breccias (left) and retrograde breccias (right) reveal chemically homogenous calcite with low concentrations of FeO, MgO and MnO. Growth bands do not record measurable chemical variations. Scale bars = 500 microns.

which may reflect variable fluid chemistry or P-T conditions during precipitation. However, consistent chemical variations were not detectable across growth zones at the level of resolution provided by the microprobe and CL banding may result from very minor variations in precipitation conditions. All infill records very low concentrations of FeO, MgO and MnO (Fig. 7.18) and chemical analyses were on the whole indistinguishable from calcite infill associated with sodic-(calcic) alteration (Fig. 7.16). Notably, the common preservation of the growth banding indicates that the calcite was not significantly recrystallized subsequent to mineral precipitation.

7.4.4 Ernest Henry ore breccia

The Ernest Henry ore breccia is characterized by predominantly moderate- to bright-luminescing calcite, and lacks growth banding (Fig. 7.19). Some samples preserve significant replacement of coarse-grained calcite by brighter-luminescing calcite along grain boundaries and twins (Fig. 7.15e). As noted above for sodic-(calcic) breccias and veins, this suggests some fluid flow after the main calcite precipitation event. Ernest Henry ore breccia calcite contains low concentrations of FeO, MgO and MnO, but with higher ratios of MnO to FeO+MgO than for other infill assemblages (Fig. 7.16). Notably, anomalous MnO concentrations are recorded immediately adjacent to some magnetite grains (Fig. 7.19). Ernest Henry magnetite has been shown to contain very high concentrations of Mn (**Chapter 6**, this study), and the enrichment in calcite MnO content adjacent to magnetite grains may reflect diffusional processes.

7.4.5 Ernest Henry marble matrix breccia

Calcite from the Ernest Henry marble matrix breccia (mmbx) has a predominantly homogeneous, moderate-luminescing CL response (Fig. 7.19b). Bright-luminescing calcite is noted along some grain boundaries, and replacing some actinolite grains. Some marble matrix breccia calcite is chemically similar to Corella formation marble calcite, but most mmbx calcite contains significantly elevated MnO concentrations (Fig. 7.16). The mmbx is relatively fine grained (most

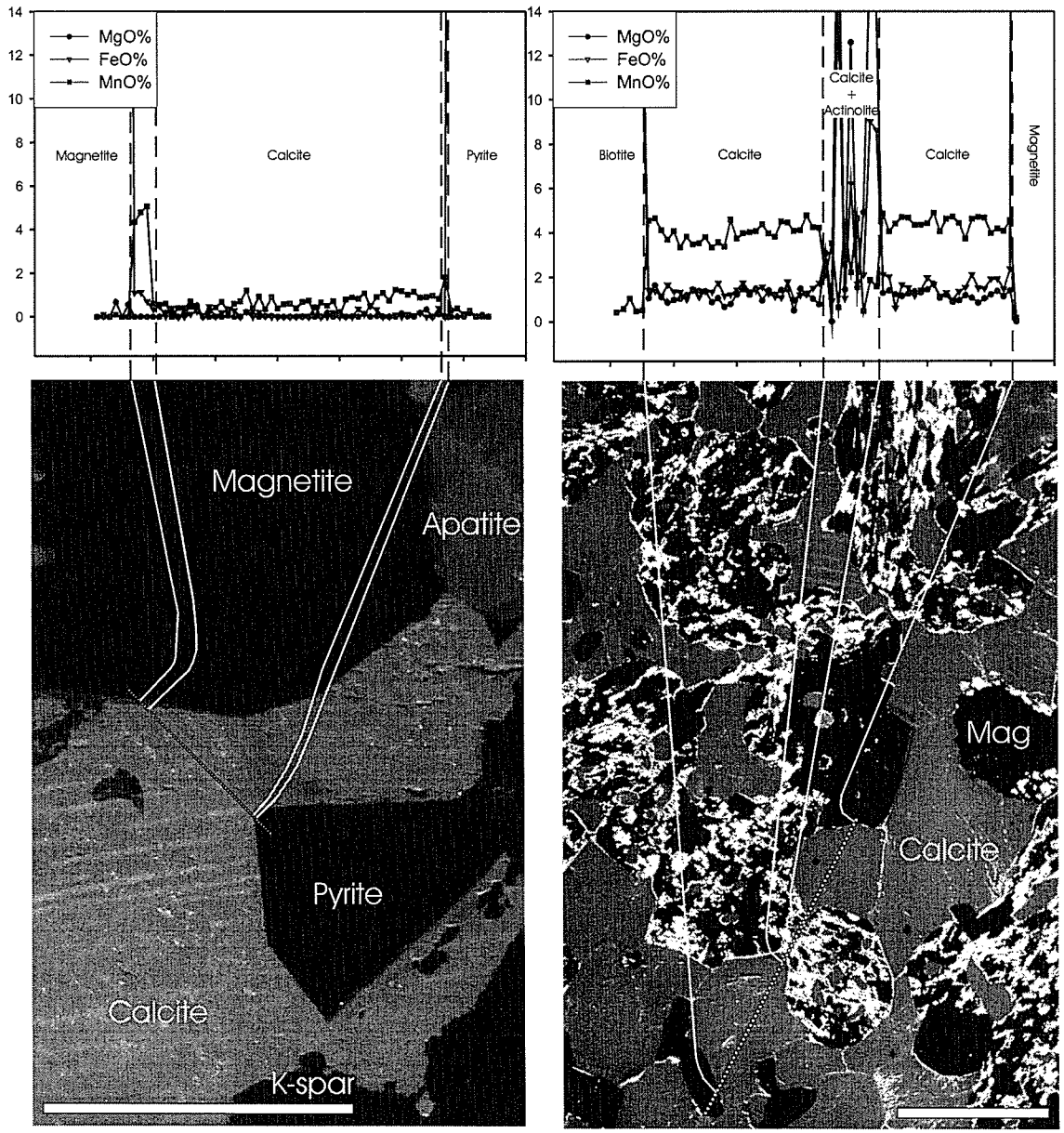

FIGURE 7.19.
CL images and microprobe traverses for calcite in Ernest Henry ore breccia (left) and Ernest Henry marble matrix breccia (right). Scale bars = 500 microns.

grains between 0.1 and 2mm) and commonly contains >10% disseminated Mn-rich magnetite. As such, the high MnO content of mmbx calcite may also reflect diffusion of Mn from magnetite into calcite. The relatively homogenous MnO content of mmbx calcite relative to ore calcite may further indicate dynamic recrystallization and homogenization of Mn concentrations during deformation.

7.5 DISCUSSION

7.5.1 Fluid pathways inferred from stable isotope ratios

Comparing the carbon and oxygen isotopic signature of the Ernest Henry footwall marble matrix breccia with Cloncurry District marbles and their altered equivalents reveals two distinct isotopic populations (Fig. 7.20). These populations may have had similar starting isotopic signatures, although unaltered marble matrix breccia is not represented in the dataset. Cloncurry District marbles converge towards values characteristic of chlorite-hematite breccias and veins, without significant shifts towards values characteristic of sodic-(calcic) breccias and veins. In contrast, the Ernest Henry marble matrix breccia converges towards isotopic values typical of sodic-(calcic) breccias and veins. These varying trends are consistent with observed mineral assemblages that reveal abundant chlorite in the altered Cloncurry District marbles, versus abundant actinolite in the marble matrix breccia. Further, networks of bright luminescing calcite are widespread in the most isotopically depleted Cloncurry District altered marble samples, but are only locally developed in the marble matrix breccia. The apparent lack of isotopic shifts in Cloncurry District marbles towards values from Cloncurry District albite-and actinolite-rich alteration assemblages suggests that the Cloncurry District marbles were not infiltrated by significant fluxes of metasomatic fluids during Na-(Ca) alteration, despite adjacent calcite-poor lithologies being intensely brecciated and metasomatised. This observation suggests that calcite-rich lithologies remained relatively impermeable during high-temperature sodic-(calcic) alteration, except in rare situations, as for the Ernest Henry marble matrix breccia, where transient permeability developed during intense shearing may have aided fluid flow and metasomatism.

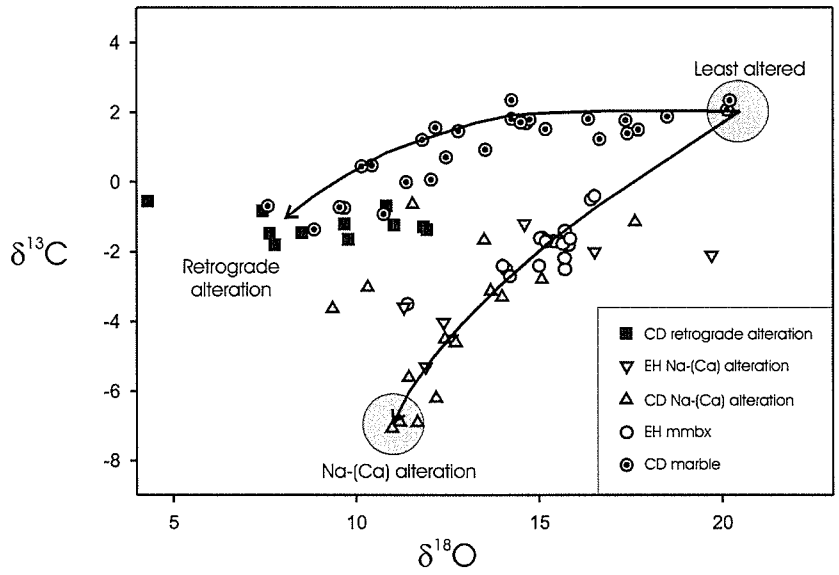

FIGURE 7.20.
Carbon and oxygen stable isotope data from Cloncurry District marbles and the Ernest Henry marble matrix breccia indicate two distinct trends with the marble matrix breccia approaching values for sodic-(calcic) alteration, and Cloncurry marbles approaching values for retrograde alteration. CD = Cloncurry District, EH = Ernest Henry, mmbx = marble matrix breccia. Arrows represent observed data variations as opposed to model curves.

These observations have important implications for the fluid flow regime during regional sodic-(calcic) alteration, and broadly synchronous Cu-Au mineralisation. Fluid flow appears to have been predominantly through fracture networks and breccias, while marbles and potentially other incompetent lithologies (e.g. schists) acted as impermeable barriers to fluid flow. Marbles are common throughout the Corella Formation, and incompetent schists are abundant within the Soldiers Cap. In these lithologies that were not prone to fracturing, through going fluid flow would have only occurred in localized zones of high strain. Thus, widespread fluid flow in fractured and brecciated Corella calc-silicates and meta-siltstones may have been focussed into more discrete fluid conduits and potential ore traps.

7.5.2 Metasomatic fluid sources

One of the principal arguments that has been used to discount magmatic fluid sources for sodic-(calcic) alteration and iron-oxide-Cu-Au mineralisation has been that the isotopic signatures of metasomatic fluids equilibrate with wallrocks along fluid flow paths, rendering interpretation of fluid sources ambiguous (e.g. Haynes, 2000). With respect to sodic-(calcic) alteration in the Eastern Succession, although shifts are noted towards progressively more rock buffered isotopic ratios as well as isotopically lighter $\delta^{18}O$ values, there is a strong clustering of data at 11‰ $\delta^{18}O$ and –7‰ $\delta^{13}C$ (Fig. 7.7). The degree of clustering of isotopic ratios indicates an isotopically homogenous fluid. The homogenous nature of this fluid is most consistent with reflecting the isotopic signature of the fluid source. Alternatively, the degree of clustering could also result from thorough isotopic equilibration of a fluid with a voluminous and isotopically homogenous rock unit that is rich in both carbon and oxygen. In the Eastern Succession, such a rock could only be represented by igneous intrusions, as meta-sedimentary rocks in both Cover Sequences 2 and 3 are out of isotopic equilibrium with the fluid of interest. However, CO_2 concentrations in magmas are typically low, and the majority of this is released into hydrothermal fluids during crystallisation, with relatively little carbon incorporated into igneous rocks (e.g. Baker, 2002). As a result, it is difficult

to explain buffering of the $\delta^{13}C$ signature of metasomatic fluids by crystalline igneous rocks, particularly for fluids that have been shown through fluid inclusion studies to contain significant CO_2 (e.g. de Jong and Williams, 1995). Thus, if non-magmatic fluids are appealed to as the predominant fluid source, and isotopic ratios are explained by interaction with magmatic bodies and metamorphic country rocks, $\delta^{13}C$ signatures should be dominated by metamorphic $\delta^{13}C$ signatures, as crystallised intrusive rocks are not likely to contain appreciable carbon. In the MKFB, there is only one main metamorphic $\delta^{13}C$ reservoir, being marine meta-carbonates of the Corella Formation. $\delta^{13}C$ values from metasomatic assemblages at ca. 1530-1520 Ma are not strongly buffered by Corella $\delta^{13}C$ signatures, implying an additional carbon reservoir. This reservoir is most consistent with CO_2-bearing fluids exsolved from crystallising plutons.

In the Cloncurry District, some rocks record $\delta^{13}C$ signatures reflecting depleted organic carbon reservoirs of black shales (Fig. 7.6). In theory, it may be possible to produce the carbon isotope values in regional sodic-(calcic) alteration by admixture of marine carbon with organic carbon. However, this possibility is not supported by the strong clustering of the data around –7‰ $\delta^{13}C$, which suggests a single reservoir rather than a mixed one. Only for those rocks in which the inferred magmatic fluid is not involved does a more convincing marine-organic mixing trend for carbon isotope ratios emerge, such as at Dugald River (Fig. 7.9). Significantly, Dugald River is a Pb-Zn-(Ag) deposit which does not share the same mineralogy, paragenesis or alteration assemblages of the other systems discussed here, and a metamorphosed syngenetic origin has been invoked by some authors (e.g. Dixon and Davidson, 1996).

Retrograde, chloritic metasomatic assemblages display low $\delta^{18}O$ values. A spread in $\delta^{13}C$ values indicates that retrograde fluids were relatively CO_2-poor (e.g. Valley, 1986), and the low $\delta^{18}O$ signature and low CO_2 content of these fluids is consistent with a meteoric origin. A lack of distinct clustering in $\delta^{18}O$ values suggests that either the fluids equilibrated significantly with host lithologies, or were mixed with fluids from other sources. The recognition of breccias and veins with 'medium temperature' or 'transitional' actinolite ± epidote ± chlorite

mineralogy in regional alteration assemblages may record mixing between saline high temperature (magmatic) and dilute low temperature (meteoric) fluids. Preliminary fluid inclusion data (Fu, in prep.) from areas such as the Gilded Rose breccia type area is consistent with this hypothesis.

Carbon and oxygen isotope data from the Mt Elliott Cu-Au deposit clusters very close to values characteristic of sodic-(calcic) alteration systems (Fig. 7.12). This, as well as similarities in mineral assemblages, suggest that fluids responsible for district-scale sodic-(calcic) alteration and Mt Elliott-style Cu-Au mineralisation were derived from similar, likely magmatic sources, and that the cores of these systems were strongly fluid-buffered. Minor shifts towards lower $\delta^{13}C$ values and slightly higher $\delta^{18}O$ values in the Mt Elliott data record minor equilibration with graphitic meta-sediments. Most data from the other Cu-Au deposits can be explained by varying degrees of equilibration between a similar external fluid originally in equilibrium with calcite $\delta^{18}O$ and $\delta^{13}C$ values of ca. 11 and –7‰ respectively, and marine meta-carbonates and graphitic metasediments. An exception to this is illustrated by the Starra (and Osborne) ironstone trend, indicating a distinct, non-magmatic, and possibly metamorphosed or metamorphogenic origin for these ironstones. Notably however, Cu-Au mineralisation at Starra post-dates ironstone formation, and isotopic data from mineralisation phases is consistent with a magmatic fluid source.

Some data, particularly from the Ernest Henry deposit, falls at $\delta^{18}O^{calcite}$ values below –11‰. As such, a meteoric fluid component cannot be ruled out, and indeed, such a source is invoked above for retrograde (chlorite-hematite) alteration in the MKFB and Cloncurry District. However, it has been shown through stable isotopes and CL images that Cloncurry District marbles record late tectonic, low temperature fluid flow that resulted in the depletion of $\delta^{18}O$ values as low as 7.5‰. CL images from Ernest Henry samples record similar late-tectonic post-mineralisation fluid flow that may have also resulted in a shift to lower $\delta^{18}O$ values. Thus while it seems likely that an isotopically light fluid, possibly of meteoric origin, is recorded by some of the Ernest Henry samples, at least some, if not all of this fluid flow post-dates mineralisation.

7.5.3 Role of fluid-wallrock interaction in Cu-Au mineralisation

All carbon and oxygen isotope data referred to in this study is plotted in Figure 7.21. Where carbonates from Cu-Au ore deposit samples are stated in their source reference as having been precipitated synchronously with ore minerals, the samples have been given distinct symbols. These syn-mineralisation carbonates exhibit a wide range in $\delta^{18}O$ and $\delta^{13}C$ ratios (Fig. 7.21). This indicates that carbon and oxygen isotopic ratios from carbonates cannot on their own be used as effective vectors towards Cu-Au mineralisation. More importantly however, the spread in data indicates that most Cu-Au ore fluids have been subject to considerable wall-rock interaction either prior to ore deposition, or at the deposition site. This observation is consistent with the model of Oliver et al. (in revision) that proposes modification of fluid chemistry by wallrock interaction as a necessary precursor to potassium-iron alteration noted in the vicinity of many Cloncurry District Cu-Au deposits (e.g. Ernest Henry, Eloise). It is also consistent with the observation of Laing (1998) that no significant Cu-Au deposits in the Eastern Succession are hosted entirely within granitic rocks, implying that fluid-wallrock interaction may be important in some of the ore deposits.

As noted above, an exception to the wide spread in isotopic data from syn-Cu-Au-mineralisation carbonates is seen in data from Mt Elliott, which contains abundant clinopyroxene in addition to magnetite, calcite, albite and sulphides. Significantly, Mt Elliott lacks abundant potassic alteration, is very close to a probable granitic fluid source, and ore assemblages are very similar to regional sodic-(calcic) alteration assemblages in the Cloncurry District and MKFB, with the addition of significant sulphide minerals and fluorite. These observations suggest that significant modification of fluid chemistry by protracted wallrock interaction may not be required for Mt Elliott-style Cu-Au mineralisation, which is essentially skarn-like.

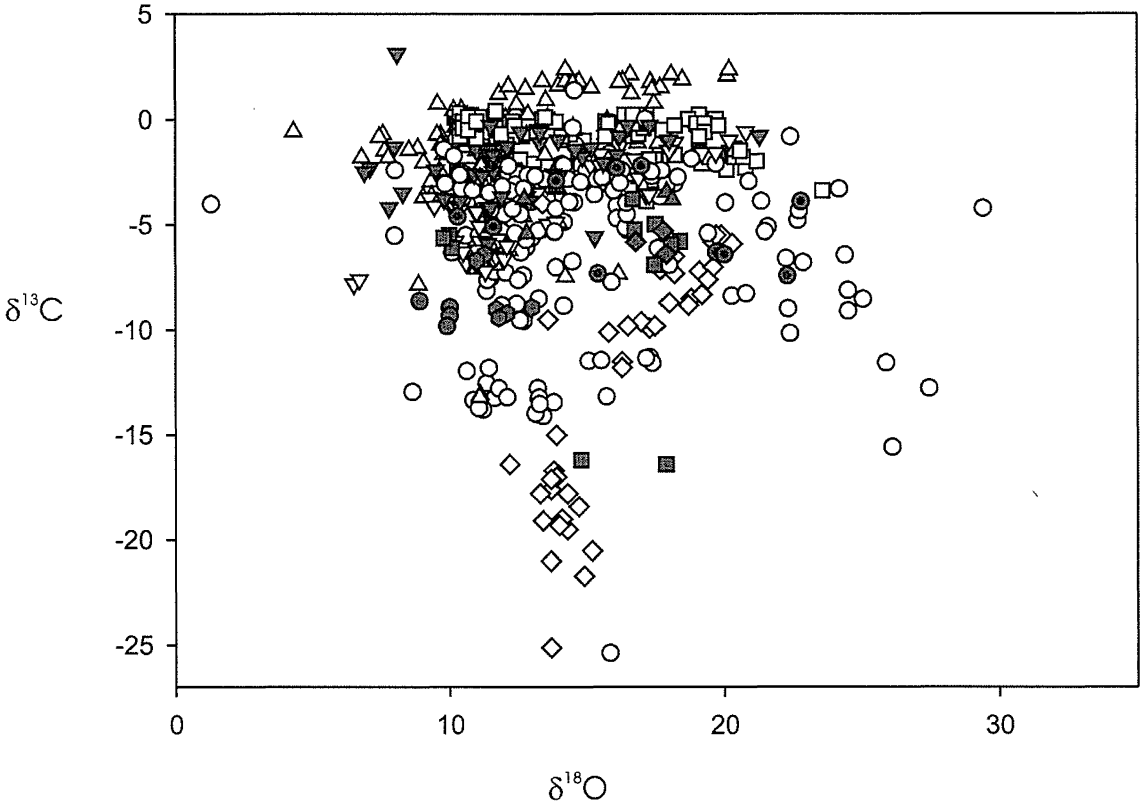

Syn-Cu-Au mineralisation	Non-mineralised or unconstrained
Great Australia	Cu-Au deposits
Starra	MKFB hostrocks and ca 1530-1520 Ma alterationon
Ernest Henry	MKFB hostrocks and ca. 1740-1730 Ma alteration
Mt Dore	Cloncurry alteration and hostrocks
Mt Elliot	Dugald River
Greenmount	
Eloise	

FIGURE 7.21.
Carbon and oxygen data for all samples presented in this study. Grey symbols are from samples that are demonstrably syn- Cu-(Au) mineralisation, while some white symbols may also be syn-mineralisation but are unconstrained from the source literature.

7.6 CONCLUSIONS

Data presented in this contribution supports a predominantly magmatic fluid source for both regional Na-(Ca) alteration and Cu-Au mineralisation in the Eastern Succession. Metamorphic fluid sources for most alteration and mineralisation assemblages are not consistent with the established isotopic signatures of the main meta-sedimentary host sequences.

As a result of complex flow paths, there is no clear $\delta^{13}C$ or $\delta^{18}O$ isotopic vector towards Eastern Succession Cu-Au mineralisation. Many syn- Cu-Au mineralisation carbonates record shifts in isotopic ratios towards those of their immediate and broader scale host sequences, and indicate that modification of fluid chemistry via fluid-wallrock interaction may be a necessary precursor for some styles of Cu-Au mineralisation in the Eastern Succession. This is particularly noted for the Ernest Henry deposit. Protracted fluid-wallrock interaction was facilitated by extensive brecciation in calcite-poor lithologies of the Corella Formation, while less competent lithologies (e.g. marbles, schists) were not prone to brecciation, and served to focus fluid flow into more discrete ore traps. In contrast to Ernest Henry, data from other deposits, most notably Mt Elliott, do not record significant shifts in isotopic ratios, and for these deposits, wallrock interaction does not appear to have been a necessary precursor to Cu-Au mineralisation.

Low temperature, CO_2-poor, $\delta^{18}O$ depleted fluids, of probable meteoric origin are involved in late stages of regional alteration, but have not contributed significantly to the oxygen and carbon budgets in the Cu-Au ore environments. As such, meteoric fluids do not appear to have played a significant role in the genesis of most Eastern Succession Cu-Au mineralisation.

Pre-mineralisation ironstones from the Starra deposit, and possibly some magnetite alteration at Osborne record distinct isotopic ratios that are inconsistent with a magmatic fluid source, whereas Starra Cu-Au mineralisation is consistent with a magmatic fluid source. This indicates the potential of non-magmatic ironstones of metamorphosed or metamorphogenic origin acting as suitable chemical hosts for Cu-Au mineralisation.

CHAPTER 7 TABLES

Table 7.1a. MKFB, C-O stable isotope data: previous sources

Location	Analyses	Rock types	Source
Calcite pods and surrounds	84	veins, breccias, marbles, calc-silicate rocks	Oliver et al. (1993)
Timberu	79	calc-silicate rocks	Cartwright (1994)
Burstall granite	50	marbles	Cartwright and Oliver (1994)

Table 7.1b. MKFB, C-O stable isotope data: this study

Sample	Location	Rock types	Mineralogy	δ18O	δ13C
T72b	Tribulation	pegmatite	alb, qtz, cal, act, chl	11.13	-6.57
T72c	Tribulation	calcite pod	cal, act, cpx, qtz, ap, ttn	10.52	-6.34
T72f	Tribulation	calcite pod	cal, act, cpx, qtz, ap, ttn	12.05	-6.02
T72i	Tribulation	calcite pod	cal, act, cpx, qtz, ap, ttn	10.18	-5.84
MP011a	Mt Philp	retrograde breccia	hem-feld, cal, qtz, chl, act, biot, mag, hem, [ep]	12.84	-3.52
MP011d	Mt Philp	retrograde breccia	hem-feld, cal, qtz, chl, act, biot, mag, hem, [ep]	11.02	-4.51
MP011d	Mt Philp	retrograde breccia	hem-feld, cal, qtz, chl, act, biot, mag, hem, [ep]	11.05	-5.09
MP022b	Mt Philp	retrograde breccia	hem-feld, cal, qtz, chl, act, biot, mag, hem, [ep]	11.62	-0.94
MP035	Mt Philp	retrograde breccia	hem-feld, cal, qtz, chl, act, biot, mag, hem, [ep]	11.02	-4.35

Oxygen and carbon isotope values reported relative to V-SMOW and PDB respectively.

Table 7.2a. Cloncurry District, C-O stable isotope data: previous sources

Location	Analyses	Rock types	Source
N. Cloncurry District	6	marbles and calc-silicate rocks	Hingst (2002)

Table 7.2b. Cloncurry District, C-O stable isotope data: this study

Sample	Location	Rock types	Mineralogy	δ18O	δ13C
BUD42-B1	Budenberri	Na-(Ca) breccia	cal, alb, act, qtz, cpx, scap, ttn, [mag]	12.18	-6.22
BUD67-B1-a	Budenberri	Na-(Ca) breccia	cal, alb, act, cpx, qtz, scap, ttn, [mag]	12.71	-4.55
BUD67-B1-b	Budenberri	Na-(Ca) breccia	cal, alb, act, cpx, qtz, scap, ttn, [mag]	12.42	-4.52
0158-B1	N. Cloncurry District	Na-(Ca) breccia	alb, cal, act, op, [ttn, biot]	10.31	-3.02
0428-B1	N. Cloncurry District	Na-(Ca) breccia	alb, act, cal, qtz, mag, [hem, ap, ttn]	11.54	-0.64
1150-B1	N. Cloncurry District	Na-(Ca) breccia	alb, cal, act, [ttn, op]	15.07	-2.79
1374-B1	N. Cloncurry District	Na-(Ca) breccia	alb, cal, qtz, act, mag, ttn	9.35	-3.64
1380b-B1	N. Cloncurry District	Na-(Ca) breccia	alb, cpx, ep, act, cal, qtz, ttn	11.18	-6.88
1380b-B1	N. Cloncurry District	Na-(Ca) breccia	alb, cpx, ep, act, cal, qtz, ttn	10.97	-7.07
0286-B2	N. Cloncurry District	retrograde breccia	hem-feld, cal, qtz, chl, op	9.79	-1.64
0345-B2	N. Cloncurry District	retrograde breccia	alb, qtz, cal, mag, [chl, pyr]	9.68	-1.20
0606b-B2	N. Cloncurry District	retrograde breccia	qtz, cal, chl, K-spar, alb, ep, ttn, op	7.63	-1.47
1214-B2-a	N. Cloncurry District	retrograde breccia	cal, qtz, hem-feld, hem, chl	7.44	-0.82
1214-B2-b	N. Cloncurry District	retrograde breccia	cal, qtz, hem-feld, hem, chl	4.30	-0.55
1375.05b-B2	N. Cloncurry District	retrograde breccia	alb, cal, qtz, chl, mag, biot, ttn, pyr, hem	11.85	-1.29
1502-B2	N. Cloncurry District	retrograde breccia	cal, qtz, plag, K-spar, chl, op, [biot, ep, rutile, ap, tourm]	10.83	-0.69
1845-B2	N. Cloncurry District	retrograde breccia	alb, qtz, cal, mag, [musc, hem]	7.77	-1.75
0029-BT	N. Cloncurry District	transitional breccia	h-feld, cal, qtz, act, [rieb, mag]	11.11	-2.77
1314-BT	N. Cloncurry District	transitional breccia	hem-feld, cal, qtz, biot, act, mag, ttn, hem, chl	9.65	-2.43
1321b-BT	N. Cloncurry District	transitional breccia	hem-feld, cal, qtz, chl, act, biot, mag, hem, [ep]	16.04	-0.28
1351a-BT	N. Cloncurry District	transitional breccia	alb, cal, qtz, act, chl, mag, hem	6.79	-1.76
1375.06c-BT	N. Cloncurry District	transitional breccia	alb, cal, qtz, mag, chl, biot, hem	16.87	-1.11
1561b-BT	N. Cloncurry District	transitional breccia	hem-feld, act, cal, hem, mag, [ttn, chl]	9.06	-2.04
1561b-BT	N. Cloncurry District	transitional breccia	hem-feld, act, cal, hem, mag, [ttn, chl]	11.00	-1.46
0082b-CS-a	N. Cloncurry District	calc-silicate rock	qtz/feld, biot, cal, op	15.95	-1.71
0082b-CS-b	N. Cloncurry District	calc-silicate rock	qtz/feld, biot, cal, op	14.41	-0.88
0086-CS	N. Cloncurry District	calc-silicate rock	cal, qtz, feld, chl, biot, [op, musc]	11.05	-0.46
0135-CS	N. Cloncurry District	calc-silicate rock	qtz/feld, cal, ep	13.99	1.60
0139-CS	N. Cloncurry District	calc-silicate rock	qtz/feld, cal, op	11.41	-1.25
0158-CS	N. Cloncurry District	calc-silicate rock	qtz/feld, act, cal, [op]	9.32	-2.96
0325-CS	N. Cloncurry District	calc-silicate rock	cal, qtz, feld, chl, biot, op	12.61	-0.88
0441-CS	N. Cloncurry District	calc-silicate rock	cal, qtz, feld, biot, [op, chl]	16.61	2.12
0607-CS	N. Cloncurry District	calc-silicate rock	feld, cal, qtz, op	9.57	0.74
0804-CS	N. Cloncurry District	calc-silicate rock	qtz, biot, cal, feld, musc, chl	10.22	-0.35
0865-CS	N. Cloncurry District	calc-silicate rock	qtz, feld, cal, biot, [op]	13.41	1.81
1375.05b-CS-a	N. Cloncurry District	calc-silicate rock	feld, qtz, cal, biot, hem	11.87	-1.39
1375.05b-CS-b	N. Cloncurry District	calc-silicate rock	feld, qtz, cal, biot, hem	11.92	-1.58
1375.09-CS	N. Cloncurry District	calc-silicate rock	cal, qtz, feld, biot, op	12.48	0.31
1375.09-CS	N. Cloncurry District	calc-silicate rock	cal, qtz, feld, biot, op	12.42	0.42
1375.10-CS	N. Cloncurry District	calc-silicate rock	cal, qtz, biot, K-spar, scap, op	17.47	0.76
1384a-CS	N. Cloncurry District	calc-silicate rock	qtz, alb, cal, act, biot, op	13.64	-3.14
1426-CS	N. Cloncurry District	calc-silicate rock	feld, cal, qtz, op	12.82	-0.75
1502-CS	N. Cloncurry District	calc-silicate rock	feld, cal, qtz, op	10.07	-1.05

Oxygen and carbon isotope values reported relative to V-SMOW and PDB respectively.

Table 7.2b. (continued)

Sample	Location	Rock types	Mineralogy	δ18O	δ13C
0036-M-a	N. Cloncurry District	marble	cal, qtz, biot	16.33	1.81
0036-M-b	N. Cloncurry District	marble	cal, qtz	10.43	0.48
0038-M-a	N. Cloncurry District	marble	cal, qtz, biot, [musc, op]	20.13	2.07
0038-M-b	N. Cloncurry District	marble	cal, qtz	14.25	1.81
0135-M-a	N. Cloncurry District	marble	cal, qtz, biot, [chl]	14.25	2.35
0135-M-b	N. Cloncurry District	marble	cal, chl	20.20	2.34
0140-M	N. Cloncurry District	marble	qtz, cal	7.58	-0.69
0282-M-a	N. Cloncurry District	marble	cal, qtz, biot, [chl, op]	12.05	0.07
0282-M-b	N. Cloncurry District	marble	cal, qtz, biot	8.85	-1.36
0352-M	N. Cloncurry District	marble	cal, qtz, hem, [chl]	11.81	1.21
0433-M-a	N. Cloncurry District	marble	cal, qtz, act	12.17	1.56
0433-M-b	N. Cloncurry District	marble	cal	10.15	0.45
0494-M-a	N. Cloncurry District	marble	cal, biot, qtz, chl, [tourm, feld, op]	9.68	-0.74
0494-M-b	N. Cloncurry District	marble	cal, biot, qtz, chl, [tourm, feld, op]	9.55	-0.72
0494-M-c	N. Cloncurry District	marble	cal, biot, qtz, chl	10.75	-0.92
0607-M-a	N. Cloncurry District	marble	cal, qtz, chl, [plag, op]	14.65	1.69
0607-M-b	N. Cloncurry District	marble	cal, qtz, chl, [plag, op]	14.74	1.79
0607-M-c	N. Cloncurry District	marble	cal, qtz, chl, [plag, op]	12.79	1.46
0865-M	N. Cloncurry District	marble	cal, qtz, biot	15.18	1.52
1047-M-a	N. Cloncurry District	marble	cal, qtz, act, biot, op	17.35	1.77
1047-M-b	N. Cloncurry District	marble	cal, [qtz, biot]	18.49	1.88
1375.09-M-a	N. Cloncurry District	marble	cal, qtz, biot, [ttn]	16.64	1.23
1375.09-M-b	N. Cloncurry District	marble	cal, qtz, biot, [ttn]	13.53	0.93
1441b-M-a	N. Cloncurry District	marble	cal, qtz, alb, K-spar, tourm	12.46	0.71
1441b-M-b	N. Cloncurry District	marble	cal, qtz, alb, K-spar, tourm	11.37	0.00
1450a-M	N. Cloncurry District	marble	cal, qtz, plag, op	14.50	1.71
0432-SC	N. Cloncurry District	Soldiers Cap	qtz, cal, [chl, op]	11.17	-2.23
1207-SC	N. Cloncurry District	Soldiers Cap	cal, qtz, graph	13.99	-4.89
1260-SC	N. Cloncurry District	Soldiers Cap	cal, alb, qtz, mag, hem	16.16	-7.32
1263-SC	N. Cloncurry District	Soldiers Cap	cal, act, graphite	8.86	-7.84
1264-SC	N. Cloncurry District	Soldiers Cap	cal, alb, act, qtz, mag, [biot]	14.22	-7.45
1266b-SC	N. Cloncurry District	Soldiers Cap	cal, alb	11.12	-13.09
1266b-SC	N. Cloncurry District	Soldiers Cap	cal, alb	11.10	-13.20
0202-V1	N. Cloncurry District	Na-(Ca) vein	cal, act, qtz, mag	13.49	-1.67
1375.04-V1	N. Cloncurry District	Na-(Ca) vein	cal, qtz, biot, act, mag	17.61	-1.14
1384a-V1	N. Cloncurry District	Na-(Ca) vein	cal, act, alb, op, qtz, ttn	13.67	-3.13
1384g-V1	N. Cloncurry District	Na-(Ca) vein	cal, qtz, alb, act, chl	13.98	-3.26
1686-V1	N. Cloncurry District	Na-(Ca) vein	cal, mag, qtz	11.43	-5.61
1714-V1	N. Cloncurry District	Na-(Ca) vein	cal, qtz, act, biot, chalcop, pyr, mag	11.67	-6.85
0286-V2	N. Cloncurry District	retrograde vein	cal, [qtz, op]	8.52	-1.45
1375.06d-V2	N. Cloncurry District	retrograde vein	qtz, pyr, cal, hem, mag, chalcop	11.94	-1.37
1506-V2	N. Cloncurry District	retrograde vein	cal, qtz, plag, k-spar, hem	11.04	-1.23
0082b-V3-b	N. Cloncurry District	rock buffered vein	cal, biot, qtz, op	17.68	-1.32
0082b-V3-a	N. Cloncurry District	rock buffered vein	cal, biot, qtz, op	14.35	-1.07
0086-V3	N. Cloncurry District	rock buffered vein	cal, qtz, biot, [op]	15.70	-0.70
0325-V3	N. Cloncurry District	rock buffered vein	cal, qtz, [biot, op, chl]	14.51	-0.35
0441-V3	N. Cloncurry District	rock buffered vein	cal, qtz	18.08	2.11
0804-V3	N. Cloncurry District	rock buffered vein	cal, qtz, op	15.75	-0.06
0865-V3	N. Cloncurry District	rock buffered vein	cal, qtz, biot	16.20	1.76
1375.09-V3	N. Cloncurry District	rock buffered vein	cal, qtz	10.40	0.20
1394-V3	N. Cloncurry District	rock buffered vein	cal, biot, qtz	13.59	0.08
1426-V3	N. Cloncurry District	rock buffered vein	cal, qtz	10.58	-1.31
1448-V3	N. Cloncurry District	rock buffered vein	cal, qtz, K-spar, alb, chl, chalcop, mag, hem, pyr, [biot]	12.87	0.24
0029-VT	N. Cloncurry District	transitional vein	cal, qtz, [hem-feld, cal, qtz, act, rib, mag]	9.05	-3.71

Table 7.3a. Ore deposits, C-O stable isotope data: previous sources

Deposit	Analyses	Commodity	Cover Sequence	Host Lithology	Source(s)
Mt Freda style	45	Au-Cu	3	TCV/MNQ	Davidson and Garner (1997)
Great Australia	12	Cu-Au-Co	2/3	TCV/CF	Davidson and Garner (1997), Cannell and Davidson (1998)
Fairstar	3	Cu-Au	3	TCV	Davidson and Garner (1997)
Monakoff	18	Cu-Au	3	TCV/MNQ	Davidson and Garner (1997)
Mt Dore	11	Cu	3	KF	Beardsmore (1992)
Starra	81	Au-Cu	3	SF	Davidson (1989), Rotherham et al. (1998)
Greenmount	15	Cu-Au	3	MS	Krcmarov (1995)
Dugald River	42	Zn-Pb-Ag	3	LCD	Porter (1990), Dixon and Davidson (1996)
Plume	6	Cu-Au	3	KF or SF	Fletcher (1999)
Houdini	4	Cu	3	SF/LCF or MNQ	Weston (2000)
Ernest Henry	59	Cu-Au	2	MFC	Twyerould (1997), Mark et al.(1999)
Osborne	5	Cu-Au	3	SF	Davidson (1989)

Oxygen and carbon isotope values reported relative to V-SMOW and PDB respectively.
TCV = Toole Creek Volcanics, MNQ = Mt Norna Quartzite, CF = Corella Formation, KF = Kuridala Formation, SF = Staveley Formation, MS = Marimo Slate, LCD = Lady Clayre Dolomite, LCF = Llewellyn Creek Formation, MFC = Mt Fort Constantine volcanics

Table 7.3b. Ore deposits, C-O stable isotope data: this study

Deposit	Sample	Commodity	Cover Sequence	Host Lithology	Syn- Cu-Au Mineralistion?	Description	δ18O	δ13C
Ernest Henry	EH.01a	Cu-Au	2	MFC	no	mmbx	15.69	-2.18
Ernest Henry	EH.01b	Cu-Au	2	MFC	yes	milled ore breccia	15.62	-2.07
Ernest Henry	EH.02a	Cu-Au	2	MFC	no	mmbx	15.02	-1.61
Ernest Henry	EH.02b	Cu-Au	2	MFC	no	mmbx	15.20	-1.68
Ernest Henry	EH.02b	Cu-Au	2	MFC	no	mmbx	15.18	-1.70
Ernest Henry	EH.02c	Cu-Au	2	MFC	yes	milled ore breccia	15.18	-1.37
Ernest Henry	EH.03	Cu-Au	2	MFC	no	Na-Ca infill	12.39	-4.03
Ernest Henry	EH.04a	Cu-Au	2	MFC	no	mmbx	15.64	-1.77
Ernest Henry	EH.04a	Cu-Au	2	MFC	no	mmbx	15.83	-1.62
Ernest Henry	EH.04b	Cu-Au	2	MFC	yes	milled ore breccia	14.85	-1.76
Ernest Henry	EH.04c	Cu-Au	2	MFC	yes	milled ore breccia	14.59	-1.43
Ernest Henry	EH.05a	Cu-Au	2	MFC	yes	milled ore breccia	11.41	-1.49
Ernest Henry	EH.05b	Cu-Au	2	MFC	yes	milled ore breccia	11.42	-1.66
Ernest Henry	EH.06	Cu-Au	2	MFC	yes	milled ore breccia	13.98	-0.99
Ernest Henry	EH07	Cu-Au	2	MFC	no	Na-Ca infill	12.62	-4.53
Ernest Henry	EH08	Cu-Au	2	MFC	no	Na-Ca infill	11.32	-3.57
Ernest Henry	EH09	Cu-Au	2	MFC	yes	milled ore breccia	8.32	-3.47
Ernest Henry	EH10	Cu-Au	2	MFC	no	mmbx	14.18	-2.68
Ernest Henry	EH10	Cu-Au	2	MFC	no	mmbx	13.98	-2.42
Eloise	EL01	Cu-Au	3	MNQ	yes	mineralised Vein	8.89	-8.56
Eloise	EL02	Cu-Au	3	MNQ	yes	mineralised Vein	9.96	-8.88
Eloise	EL03	Cu-Au	3	MNQ	yes	mineralised Vein	9.98	-9.28
Eloise	EL04	Cu-Au	3	MNQ	yes	mineralised Vein	9.85	-9.79
Eloise	EL04	Cu-Au	3	MNQ	yes	mineralised Vein	9.91	-9.76
Mt Elliott	ME01	Cu-Au	3	KF	yes	breccia infill	11.71	-9.00
Mt Elliott	ME01	Cu-Au	3	KF	yes	breccia infill	12.08	-9.16
Mt Elliott	ME02	Cu-Au	3	KF	yes	breccia infill	12.95	-8.89
Mt Elliott	ME03	Cu-Au	3	KF	yes	breccia infill	11.30	-6.44
Mt Elliott	ME03	Cu-Au	3	KF	yes	breccia infill	10.95	-6.68
Mt Elliott	ME04	Cu-Au	3	KF	yes	breccia infill	11.80	-9.38

Oxygen and carbon isotope values reported relative to V-SMOW and PDB respectively.
MNQ = Mt Norna Quartzite, KF = Kuridala Formation, MFC = Mt Fort Constantine volcanics

Table 7.4 Strontium isotope data

Sample	Rock Type	Area	$^{87}Sr/^{86}Sr$	2 σ error	Sr (ppm)	Rb (ppm)	$^{87}Rb/^{86}Sr$	Calculated $^{87}Sr/^{86}Sr_{initial}$ 1500Ma	1550Ma	1760Ma
1450a-M	marble	CD	.709826	14	175.3	0.173	.002856	.709765	.709762	.709754
1047-M-a	marble	CD	.711086	17	158.4	0.054	.000985	.711064	.711064	.711061
038-M-a	marble	CD	.709334	15	221.5	0.199	.002594	.709279	.709277	.709269
BUD42-B1	sodic breccia	CD	.712159	46	19.9	0.015	.002246	.712111	.712109	
1384a-CS	sodic vein	CD	.712625	19	71.4	0.348	.014124	.712321	.712311	
T72c	sodic vein	MKFB	.739768	30	17.0	0.082	.013957	.739467	.739457	
1351a-BT	retrograde breccia	CD	.722327	40	7.5	0.056	.021645	.721861	.721845	
0345-B2	retrograde breccia	CD	.718510	51	11.7	0.020	.004928	.718404	.718401	
EH09	ore breccia	EH	.719832	18	20.7	0.035	.004869	.719727	.719724	
EH10	mmbx	EH	.714408	12	66.3	1.016	.044321	.713454	.713422	.713286

CD = Cloncurry District, MKFB = Mary Kathleen Fold Belt, EH = Ernest Henry

SYNTHESIS AND CONCLUSIONS

SYNTHESIS AND CONCLUSIONS

8.1 INTRODUCTION

The Eastern Succession of the Mt Isa Block contains numerous examples of Fe-oxide-Cu-Au mineralisation and research in this district has played a key role in the development of genetic models for this class of mineralisation. This thesis has employed a combination of structural and geochemical tools in an attempt to clarify the role of regional scale brecciation and metasomatism in mineralisation processes, with particular emphasis within Mary Kathleen Group stratigraphy of the Cloncurry District. The following is a summary and synthesis of the key outcomes of this investigation, as well as implications for exploration, and suggestions for future research directions.

8.2 STRUCTURAL FRAMEWORK

Structural observations in the Cloncurry Region as well as the Budenberri, Tribulation – Lime Creek and Mt Philp areas are largely consistent with a protracted history of predominantly E-W directed compression. This history includes D_1 emplacement (thrusting?) of Cover Sequence 3 rocks over Cover Sequence 2 rocks, and subsequent D_2 tight to isoclinal folding. Variations in D_2 fold geometry reflect a combination of reactivation of early formed faults either syn- or post-D_2, strain partitioning around early intrusive bodies, forceful displacement of wallrocks during emplacement of the Williams and Naraku batholiths, and local refolding during D_3 (**Chapter 2**). Recognition of these effects indicates that most broad scale variations in fold patterns do not require multiple shifts in the regional shortening direction, and can be explained within in a coherent tectonic framework, as proposed by O'Dea et al. (1997) and MacCready et al. (1998).

With the exception of the Osborne deposit, most significant occurrences of Cu-Au mineralisation in the Eastern Succession appear to have formed during the waning phases of the Isan Orogeny, and during broadly E-W directed D_3 shortening. However, on a local scale shortening direction varied significantly during D_3, with for example, SSE-NNW directed shortening inferred in the Gilded Rose area, and

E-W directed shortening in the Tribulation – Lime Creek area. Establishing the specific causes for local variations in shortening direction is an arduous task fraught with ambiguity, but is not essential from an exploration perspective. However, given the importance of dilational zones within faults and shears in hosting Cu-Au mineralisation in the Eastern Succession, establishing local shortening directions and determining optimal fault orientation for dilation is critical in targeting favorable fault segments for mineralisation.

8.3 WIDESPREAD BRECCIATION IN THE CORELLA FORMATION

Regional mapping has confirmed the extremely widespread distribution of brecciation within Mary Kathleen Group stratigraphy of the Cloncurry District. For example, in the Cloncurry Region, greater than 50% of exposed Corella Formation stratigraphy is fractured and brecciated to varying degrees (Fig. 4.2). In the MKFB, and in portions of the Cloncurry District where stratigraphy had a predominant N-S trend at the onset of D_3, broadly E-W directed shortening was primarily accommodated by reactivation of D_2 structures, as opposed to refolding, and in these areas, brecciation is poorly developed. Brecciation in the MKFB is largely confined to discrete shear and fault zones, and to strain shadows around competent pre-metamorphic intrusive bodies (e.g. Oliver et al., 1990).

Where D_3 folding occurred within the Corella Formation, it was imposed on rocks that were fractured and boudinaged both pre- and syn-D_3, producing chaotic breccia-like arrangements of boudins or clasts. Competent, calcite-poor lithologies within the Corella Formation record negligible hinge thickening and limb thinning during D_3 folding, and folding of these layers resulted in space problems. Locally, space problems were accommodated by increased flow of incompetent calcite-rich lithologies towards fold hinges. Additionally, brecciation resulted in a net reduction in the competence of some originally stiff layers, allowing for increased flow and the accommodation of some buckle fold related space problems (**Chapter 4**). Syn-folding fracturing and brecciation may have been facilitated in part by volume gain folding and effective layer thinning, proposed variations on models of tangential longitudinal strain (**Chapter 3**).

A morphological continuum has been documented between rotated boudins, fractured multilayers, and stratabound breccia bodies, implying a genetic link between boudin rotation, cataclasis and brecciation processes. Rotation of boudins in single layers is well documented, and it is inferred here that shear stress acting obliquely across stratigraphic layering resulted in rotation of clasts in crackle brecciated multilayers causing cataclasis, and producing both stratabound and discordant breccia bodies (**Chapter 4**).

Contributing factors for D_3 brecciation in the Corella Formation of the Cloncurry District include:

1) Lower D_2 temperatures in the Cloncurry District relative to the MKFB, promoting late- D_2 fracturing and boudinage;
2) A range in fold orientations in the Cloncurry District at the onset of D_3, favoring widespread refolding, as opposed to predominant tightening of D_2 folds in the MKFB;
3) Lower temperatures of D_3 relative to D_2, which a) enhanced competence contrasts between calcite-poor and calcite-rich lithologies, leading to the development of buckle fold related space problems, and b) favored reactivation of D_2 fractures and propagation of D_3-fractures and brecciation;
4) Large competence contrasts between calcite-rich and calcite-poor lithologies in the Corella Formation, with brecciation occurring in sequences with a low proportion of marbles; and
5) Inferred elevated fluid pressure and strain rate associated with voluminous pluton emplacement.

While fracturing and brecciation were widespread in Corella Formation siltstones, calcite-rich marbles were not prone to the development of through going brittle fractures. Further, mineral assemblages and stable isotope data indicate that most marbles remained relatively impermeable during high temperature Na-(Ca) metasomatic events (**Chapter 7**), with albite- and actinolite-rich alteration assemblages recording fluid flow predominantly through fracture networks and breccia bodies developed in more competent lithologies. The occurrence of

interlayered low competence and low permeability calcite-rich layers within the Corella Formation would have had a significant influence on the fluid flow regime during pluton emplacement and associated Na-(Ca) metasomatism. A scenario can be envisaged in which low permeability marble horizons isolated high permeability fracture networks from one another (Fig. 8.1a). Incompetent schists in the Soldiers Cap Group were also not prone to brittle failure. Given the broader structural geometry of the Cloncurry District, with the Soldiers Cap Group overlying much of the Mary Kathleen Group, low permeability rocks in the Soldiers Cap Group may have served as a largely impermeable cap overlying widespread brecciation in the Corella Formation (Fig. 8.1a).

8.4 DILATIONAL FAULT ZONE CHARACTERISTICS

Dilational fault zones are amongst the most important epigenetic ore hosts in the Cloncurry District and elsewhere. The nature of breccias and veins developed within dilational fault zones depends in large part on the vertical continuity of the zone of dilation, and the permeability of surrounding rocks (**Chapter 5**). For example, the genesis of large aperture veins (>1m width) is argued to be dependent on expansion of originally small fractures by hydraulic expansion, a process that requires zones of locally decreased mean stress and increased permeability. Fluid pressure must remain high in order to force wallrocks apart, and while these veins have been documented within strike-slip faults, irregularities in the fault plane may have prevented vertically continuous dilational zones from developing. In contrast, fluidization and gas streaming require large fluid pressure gradients to drive rapid and sustained fluid flow. Consequently, these processes are favored in vertically continuous dilational zones, particularly where such zones span the transition from near lithostatic fluid pressure at depth, to near hydrostatic fluid pressure at shallow levels (Fig. 8.1b).

In general, the development of vertically continuous zones of dilation is favored in strike-slip faults, and to a lesser degree in normal faults, as opposed to reverse faults, and is further promoted by large magnitude fault slip, steep fault geometries, and long and steeply oriented fault jogs. As such, clast transport in the

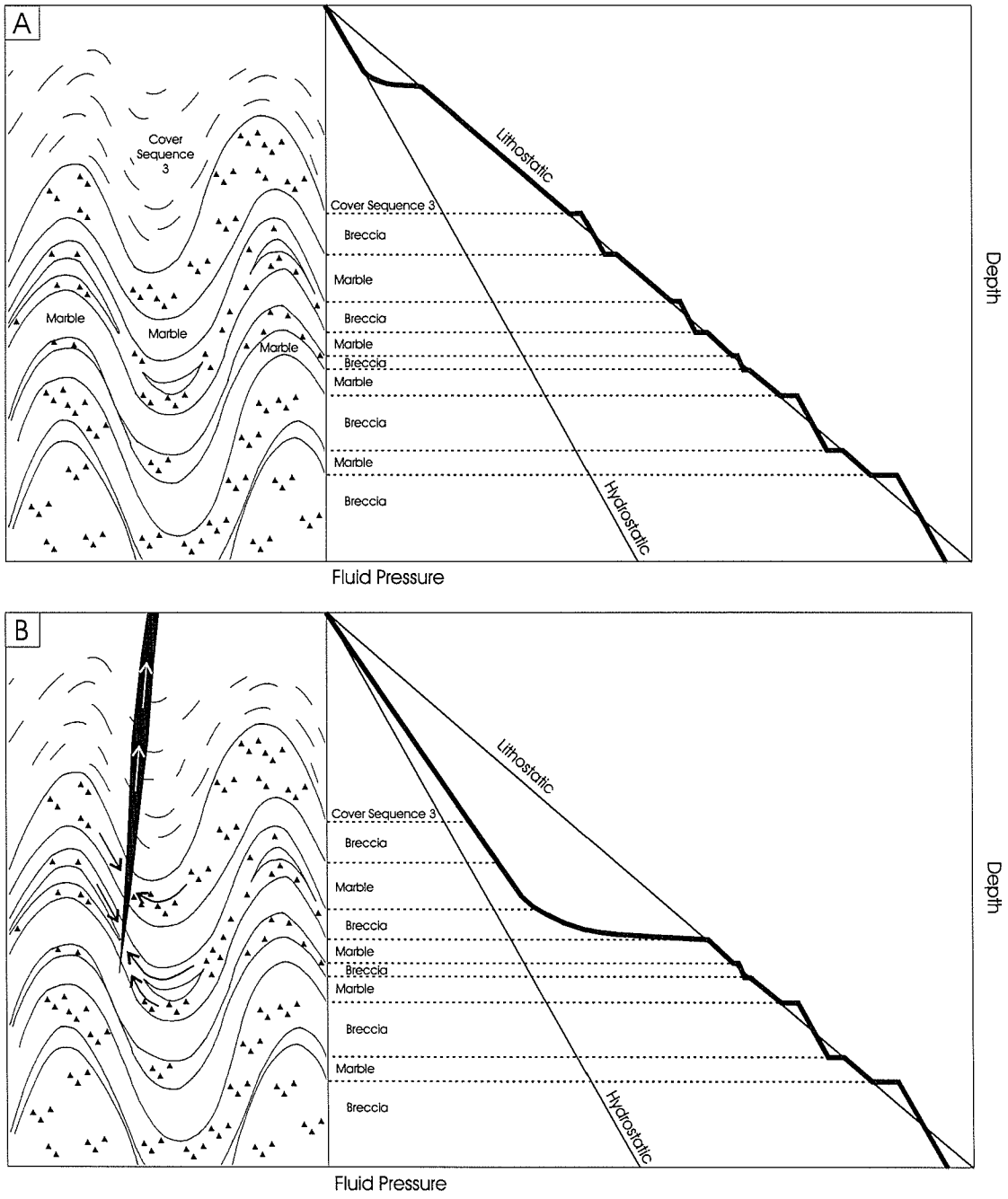

FIGURE 8.1.
(a) Schematic cross-section of widespread brecciation in competent layers within the Corella Formation, separated by intact, low permeability marble horizons, and capped by non-brecciated, low permeability lithologies within Cover Sequence 3. Fluid pressure within highly permeable brecciated sequences may approach hydrostatic gradients (albeit at near lithostatic values). (b) Where throughgoing fault zones breach low permeability barriers to fluid flow, significant pressure drops may result in catastrophic fault valving, with voluminous fluid flow from originally separated, stacked fracture-breccia networks towards and up fault zones.

Gilded Rose breccias by inferred gas streaming may have been favored by a district scale temporal shift from compressional to wrench tectonics (e.g. O'Dea et al., 1997). Also, breaching of low permeability barriers to fluid flow, and resultant catastrophic fluid release was likely aided by fluid overpressures resulting from emplacement and crystallization of the Williams and Naraku batholiths. Notably however, pluton emplacement may have been facilitated by a district scale shift from compression to transtension.

Large fluid fluxes into dilational fault zones are favored where faults are emplaced into fluid overpressured, high permeability zones, including for example fracture and breccia networks. As argued in this thesis, such networks were widespread in the Corella Formation of the Cloncurry District, and interleaved low permeability marbles may have allowed for stacking of such networks over large depth intervals. This scenario would have provided a large volume of rock out of which fluid could have been sourced during fault valving (Fig. 8.1b). Notably, repeated fault valve action at the same locale would only be favored where faults are severely misoriented for reactivation, allowing for the attainment of widespread elevated fluid pressures between fault slip episodes. Further, overpressured fluids are difficult to maintain in extensional tectonic regimes (Sibson, 2001), and as such, local extensional zones developed within a broader compressional or transtensional tectonic setting as a result of stress partitioning may serve to draw large fluid volumes into discrete structural zones. This appears to have been the case at Ernest Henry, where Coward (2001) interpreted kinematic indicators consistent with normal slip on controlling shear zones.

8.5 METASOMATIC FLUID SOURCES

Most recent researchers in the Eastern Succession have favored magmatic fluid sources for widespread Na-(Ca) alteration, ore-proximal K-Fe alteration and Cu-Au mineralisation. A similarity in mineral assemblages and mineral chemistry between inferred magmatic-hydrothermal transition assemblages, and broader Na-(Ca) metasomatic assemblages, as well as a compilation of new and previously published oxygen isotope data (**Chapter 6**) are also consistent with inferred

magmatic fluid sources. However, arguments have been raised by other authors (e.g. Haynes, 2000) that fluid oxygen isotope ratios are readily reset by equilibration with lithologies along the fluid flow path, and as such do not necessarily reflect the ultimate fluid source. In order to confidently discriminate between fluids exsolved from crystallizing magmatic rocks, and fluids of other sources that have equilibrated with igneous rocks, isotopic or geochemical tracers must be employed that are not easily reset by equilibration with igneous rocks.

In this thesis, a combined carbon, oxygen and strontium isotopic investigation of carbonate minerals has been undertaken (**Chapter 7**). Although this approach does not appear to be directly applicable as a vector towards mineralisation, it has proved extremely useful in confidently characterizing metasomatic fluid sources, and in documenting the effects of fluid-wallrock interaction. Because of the low concentration of carbon in most igneous rocks, the carbon isotopic signature of CO_2-rich metasomatic fluids is not easily reset by interaction with igneous rocks. The strong clustering of $\delta^{13}C$ and $\delta^{18}O$ values from the cores of Na-(Ca) alteration systems at –7 and 11‰ respectively is most consistent with fluids exsolved from crystallizing intrusions. Data from Cu-Au mineralisation also clusters around $\delta^{13}C$ and $\delta^{18}O$ values of –7 and 11‰ respectively, consistent with a similar, magmatic fluid source. Significant spread is seen in ore proximal carbonate samples, reflecting equilibration between metasomatic fluids and different host rocks, including marine meta-carbonates and graphitic metasediments. In contrast, retrograde metasomatic mineral assemblages record low $\delta^{18}O$ signatures that indicate a component of cooler, low $\delta^{18}O$, low X_{CO2} fluid, of inferred meteoric origin.

Future investigations into the sources of metasomatic fluids in the Eastern Succession should build on the isotopic databases compiled and presented in this study. In particular, preliminary strontium isotope analyses have yielded encouraging results, and future studies would benefit greatly from strontium isotope characterization of various host rock sequences, by means of whole rock strontium isotopic analysis of least altered lithologies. With respect to carbon and oxygen isotopes, little data exists from the Osborne deposit, and additional analyses could

do much to shed light on the genesis of this enigmatic deposit. An additional possibility for metasomatic fluid tracers are Br/Cl ratios of metasomatic fluid inclusions, and although not investigated in this study may prove useful in future investigations of fluid sources in the Cloncurry District.

8.6 METAL AND LIGAND SOURCES

The source of metals for Cloncurry District Fe-oxide Cu-Au mineralisation has not been directly investigated within the scope of this thesis. However, concurrent work by Oliver et al. (in revision) proposes that some ore system components, and in particular K and Fe, may be stripped from wallrocks during regional alteration, and later precipitated in ore environments. The structural scenario outlined in this thesis, whereby metasomatic fluids had access to large volumes of brecciated rocks, and were then focussed into more discrete conduits would certainly favor the model of Oliver et al. (in revision). Further, isotopic data suggests that for some Cloncurry District deposits and for the Ernest Henry deposit in particular, fluid-wallrock interaction played a significant role in modifying fluid (isotopic) chemistry prior to mineralisation. However, fluid inclusion data from some igneous hosted metasomatic assemblages (e.g. Lightning Creek; Perring et al., 2000) indicates that some inferred magmatic fluids were already K-, Fe-, and Cu-rich upon exsolution from their parent melt. Clearly more work can be done in better constraining metal sources, and ongoing fluid inclusion work (e.g. Fu, in prep.) should prove most useful in this respect. Also, direct analysis of isotopic ratios of ore components including Cu and Fe may prove fruitful as these techniques become more commonplace.

In some Fe-oxide-Cu-Au districts, the saline nature of inferred surficial fluids is thought to reflect fluid derivation from playa lakes, or by leaching salts from evaporite sequences (e.g. Barton and Johnson, 1996). Mixing of such brines with hotter, and possibly magmatic fluids has been invoked as a critical ore forming mechanism for some examples of Fe-oxide-Cu-Au mineralisation (e.g. Haynes et al., 1996). However, this does not appear to be the case in the Cloncurry District, where meteoric fluids are paragenetically late, and based on stable isotope data, do

not appear to have contributed significantly to ore processes. Further, ongoing fluid inclusion studies (e.g. Fu, in prep.) indicate that meteoric fluids in the Cloncurry District were neither saline nor metal rich. The dilute nature of meteoric fluids in this district may indicate that the fluids were neither hot enough, nor saline enough to strip significant concentrations of ligands or ore components from evaporite sequences that were already metamorphosed at greenschist to amphibolite facies conditions. In contrast, the possibility has been raised in this thesis of hot and already saline magmatic fluids becoming progressively enriched in chlorine through fluid-wallrock interaction, and the breakdown of chlorine-bearing metamorphic minerals within the evaporitic Corella Formation. This concept has only been touched on in the present study, and clearly warrants further work, through for example additional analysis of chlorine concentrations in hydrous minerals (e.g. microprobe analysis), fluid inclusions (e.g. PIXE analysis) and whole rock samples (e.g. Neutron activation analysis). The above data could serve as the basis for rigorous mass balance calculations in order to assess the potential contribution of evaporitic chlorine to metasomatic systems.

8.7 STRUCTURAL AND GEOCHEMICAL SYNTHESIS

A scenario has been established in this thesis where fluids exsolved from voluminous intrusions of the Williams and Naraku batholiths had access to large volumes of rock, particularly in the Corella Formation. Fluid flow was predominantly through fracture and breccia networks, while lithologies that were not prone to throughgoing brittle failure acted as low permeability barriers to fluid flow. These low permeability horizons allowed elevated fluid pressures to be maintained in greater volumes of rock than would have been otherwise possible. Widespread fluid flow is recorded by alteration of a variety of host rocks towards Na-(Ca)-rich metasomatic assemblages. Widespread brecciation was likely faciliated by elevated fluid pressures associated with pluton emplacement and crystallisation.

A shift from widespread mixed brittle-ductile deformation towards more focussed brittle deformation likely reflects progressive cooling during the waning

phases of the Isan Orogeny, as well as locally elevated fluid pressure and/or strain rate. This shift served to focus widespread fluid flow into more discrete conduits. These conduits are particularly noted in stratigraphic sequences other than and structurally higher than the Corella Formation, where metasomatic rocks are spatially restricted relative to within the Corella Formation. Notably, with the exception of Ernest Henry, all significant late-metamorphic Cu-Au deposits in the Cloncurry District (e.g. Eloise, Mt Elliott, Starra, Greenmount, Mt Dore, and Great Australia) are hosted within Cover Sequence 3 stratigraphy. Further, the Ernest Henry deposit is not hosted within typical calc-silicate rocks of the Corella Formation, but predominantly within a thick sequence of Mt Fort Constantine felsic volcanic rocks. Thus it is hypothesized that in much of the Corella Formation of the Cloncurry District, metasomatic fluid conduits were simply too widespread and diffuse in order to serve as effective ore hosts. In contrast, catastrophic fault valving, whereby fluids were sourced out of large volumes of brecciated Corella Formation stratigraphy and focussed into discrete conduits in overlying stratigraphic sequences, may have provided an ideal scenario for mineralisation. This focussing of fluid flow would have also had the potential to lead to mixing of fluids of different sources, as proposed for example as a precipitation mechanism at Ernest Henry (Mark et al., 1999). Additionally, pressure fluctuations associated with fault valve behavior would be expected to lead to rapid unmixing of H_2O-CO_2-NaCl fluids, affecting equilibrium mineral assemblages (e.g. Pollard, 2001) and leading to the precipitation of minerals with pressure sensitive solubilities. Further, geochemical traps for mineralisation are arguably more common within Cover Sequence 3, and include reduced stratigraphic sequences (e.g. metamorphosed black shale horizons) and early iron-rich formations, including inferred syngenetic ironstones (e.g. Starra ironstones; Davidson, 1989). Focussed flow of oxidised and metal-rich fluid towards such traps provides an important ore precipitation mechanism.

A further consequence of a shift towards throughgoing fault zones is that these appear to have allowed for the introduction of dilute surface derived fluids into Eastern Succession hydrothermal systems. While these fluids do not appear to

have played in significant role in mineralisation, they have apparently mixed with hotter saline fluids of magmatic origin and resulted in widespread lower temperature and paragenetically late metasomatic assemblages (Transitional to Retrograde assemblages; **Chapters 6 and 7**).

8.8 FE-OXIDE-CU-AU CLASSIFICATION

Various authors have presented a number of schemes for the classification of Cloncurry District Cu-Au mineralisation (e.g. Williams, 1998; Mark et al., 2001). The following scheme is based on these earlier classifications, and hinges in large part on recognition of the role of host rocks in affecting the geochemical and resultant mineralogical characteristics of deposits. The structural and stratigraphic setting of the following deposit types in relation to widespread brecciation in the Corella Formation is illustrated schematically in Figure 8.2.

8.8.1 Mt Elliott-style deposits

Mt Elliott-style deposits include the Mt Elliott Cu-Au deposit (Little, 1997) and the SWAN (Pollard et al., 1997c) and Brumby (Foster, 1995) prospects. These deposits are characterized by skarn-like Na-(Ca)-rich metasomatic assemblages (e.g. actinolite-, pyroxene-, scapolite- and albite-rich assemblages) that were precipitated together with Cu-sulphides, Fe-oxides and gold. Isotopic signatures from Mt Elliott are consistent with magmatic-derived metasomatic fluids that record negligible interaction with host rocks en-route to the deposition site, although the carbonaceous nature of the immediate host rocks to mineralisation at Mt Elliott may have facilitated precipitation of sulphide minerals. The deposits are proximal to large intrusive bodies, and fluid flow from inferred magmatic sources was focussed into appropriate structural sites including dilational fault jogs. Mt Elliott-style deposits show both geochemical and structural similarities with 100s of large aperture calcite-rich veins developed throughout the Eastern Succession, and indicate the potential for Na-(Ca) metasomatic systems to directly precipitate economic concentrations of Cu and Au.

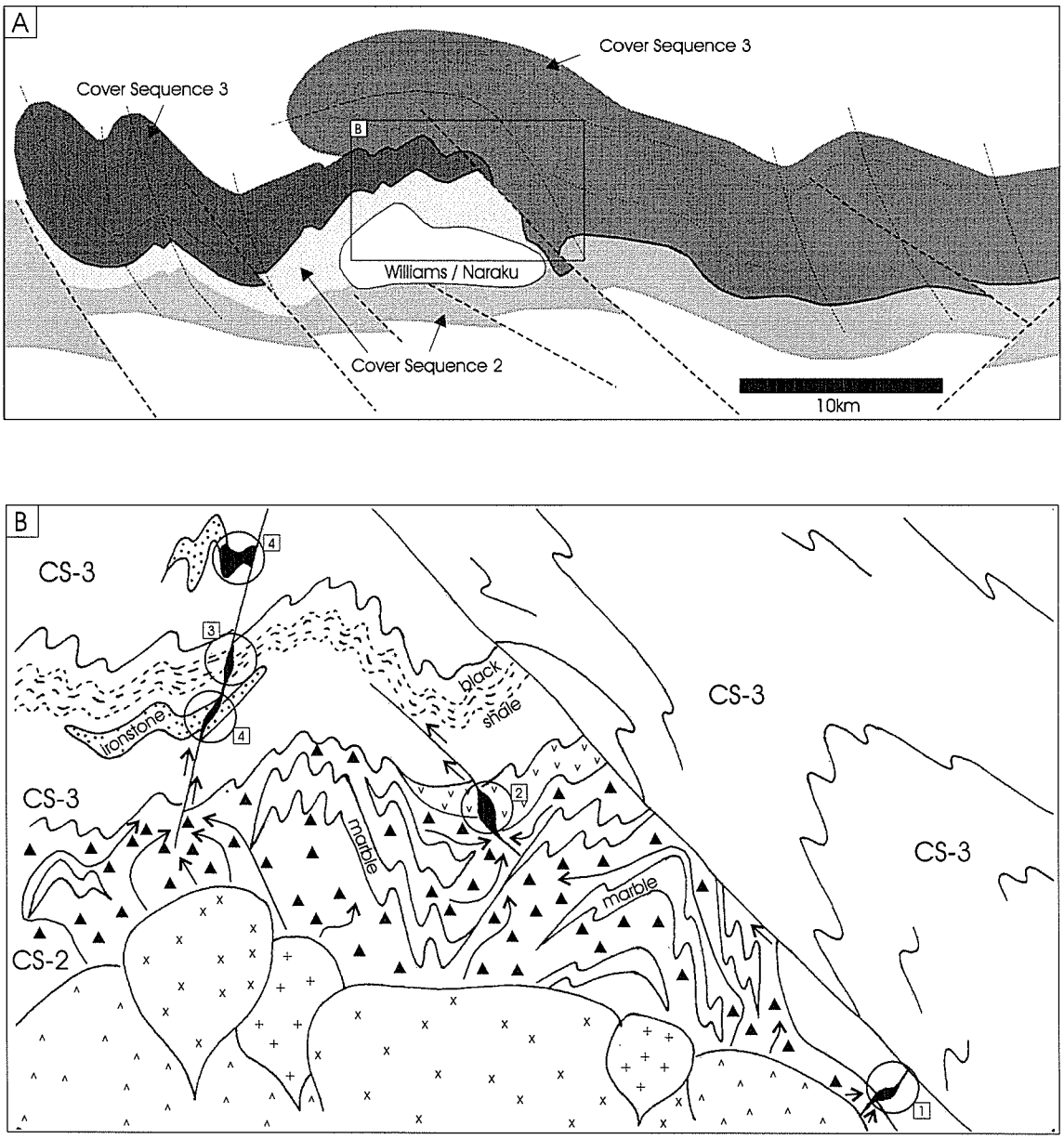

FIGURE 8.2.
(a) Schematic E-W cross section of the Cloncurry District, modified after Giles and MacCready (1997). (b) Enlargement of an area indicated in Figure 8.2a, schematically illustrating the structural and stratigraphic setting of various styles of late metamorphic Cu-Au mineralisation in the Cloncurry District: 1) Intrusion proximal, Mt Elliott-style deposits. 2) Intrusion distal, Ernest Henry-style deposits. 3) Reduced Cu-Au deposits hosted within broader reduced stratigraphic sequences, including for example carbonaceous black shales. 4) Pre-mineralisation ironstone hosted Starra-style Cu-Au deposits. Arrows represent possible fluid flow paths pre- and syn-mineralisation. CS-2 = Cover Sequence 2, CS-3 = Cover Sequence 3.

8.8.2 Ernest Henry-style deposits

The Ernest Henry deposit formed distal to any known synchronous intrusive bodies, and is localized by a dilational shear flexure within a thick sequence of felsic volcanic rocks. The large competence contrast between this sequence and the underlying calcite-rich marble matrix breccia may have helped focus dilation and mineralisation at this locale. Ernest Henry-style deposits are characterized by Cu-sulphides and gold precipitated synchronously with K- and Fe-rich metasomatic assemblages, including biotite, K-feldspar and magnetite. Cloncurry District prospects that exhibit similar K- and Fe- rich metasomatic assemblages include Mt Dore (Beardsmore, 19992) and Greenmount (Krcmarov, 1995). The K- and Fe-rich character of the Ernest Henry deposit has been inferred by Oliver et al. (in revision) to reflect extensive fluid wallrock equilibration prior to ore precipitation. This model is supported by isotopic data that records shifts toward $\delta^{18}O$ and $\delta^{13}C$ values characteristic of Corella Formation marine metacarbonates. While Mt Elliott style deposits described above indicate that extensive fluid-wallrock equilibration is not a necessary precursor for all styles of Cu-Au mineralisation in the Cloncurry District, such equilibration appears to be important in the genesis of Ernest Henry-style mineralisation. Notably Ernest Henry is the largest Cu-Au deposit in the region.

8.8.3 Reduced Cu-Au deposits

Eloise is the best-documented example of reduced Cu-Au mineralisation in the Cloncurry District (Baker, 1998), with other examples including the Lady Clayre (Haberman, 1999), Fairstar (Davidson and Garner, 1997) and Greenmount (Krcmarov, 1995) prospects. Mineralisation at these deposits is associated with little or no Fe-oxide, while pyrrhotite is a common gangue mineral. As emphasised by Haynes (2000) reduced mineral assemblages in these deposits relative to Fe-oxide rich deposits in the same district likely reflect the reduced nature of broader hostrocks to the deposits, which commonly contain carbonaceous schists. Some reduced Cu-Au deposits are hosted within broader zones of K-Fe-metasomatism, manifest in the case of Eloise by extensive hornblende- and biotite-rich alteration, and may reflect similar processes to Ernest Henry-style mienralisation.

8.8.4 Starra-style deposits

Starra-style deposits are characterized by Cu-Au mineralisation that is largely hosted by earlier magnetite-rich ironstones. The origin of ironstones at Starra is controversial, with both syngenetic (e.g. Davidson, 1989) and epigenetic (e.g. Rotherham et al., 1997) models having been proposed. In contrast, fluids responsible for Cu-Au mineralisation at Starra appear to be magmatic in origin (Rotherham, 1998; **Chapter 7**, this study). Some pre-mineralisation ironstones of possible syngenetic origin have also been documented at Monakoff and Osborne, (Davidson and Davis, 1997; Banvill, 1998). Notably however the sources Cu and Au bearing fluids in these deposits, and particularly at Osborne (see below) remain controversial.

8.8.5 Osborne-style deposits

Cu-Au mineralisation at Osborne has recently been shown to have occurred at ca. 1595 Ma, broadly synchronous with peak metamorphism and D_2 deformation (Gauthier et al., 2000). While the deposit exhibits a skarn-like mineralogy (Gauthier et al., 2000), no voluminous intrusions of this age have been documented in the Cloncurry District, although peak-metamorphic partial melting is evident in the vicinity of Osborne (Rubenach et al., 2000). Clearly the origin of mineralisation at Osborne remains contentious, and a metamorphosed or metamorphogenic origin cannot be ruled out.

8.9 SUMMARY

With the notable exception of the enigmatic Osborne deposit, most examples of Cu-Au mineralisation formed broadly synchronously with emplacement of the Williams and Naraku batholiths and associated widespread Na-(Ca) metasomatism. Metasomatic fluids gained access to large volumes of host rocks through fracture and breccia networks, the development of which was facilitated by pluton emplacement and by heterogeneous shortening of an already structurally complex terrane. The wide variety in Cu-Au mineralisation styles can be attributed to

variations in structural and stratigraphic position and the degree of fluid modification by wallrock interaction prior to ore precipitation. While widespread brecciation and metasomatism was not a necessary precursor in all styles of mineralisation, some deposits, and Ernest Henry in particular, record modification of fluid chemistry that was facilitated by widespread brecciation in the Corella Formation.